



# Velocity–conductivity relationships for mantle mineral assemblages in Archean cratonic lithosphere based on a review of laboratory data and Hashin–Shtrikman extremal bounds

Alan G. Jones <sup>a,\*</sup>, Rob L. Evans <sup>b</sup>, David W. Eaton <sup>c</sup>

<sup>a</sup> Dublin Institute for Advanced Studies, 5 Merrion Square, Dublin 2, Ireland

<sup>b</sup> Department of Geology and Geophysics, Woods Hole Oceanographic Institution, Woods Hole, Massachusetts 02543, USA

<sup>c</sup> Department of Geoscience, University of Calgary, Calgary, Alberta, Canada T2N 1N4

## ARTICLE INFO

### Article history:

Received 13 August 2007

Accepted 22 October 2008

Available online 5 November 2008

### Keywords:

Archean lithosphere

Seismic velocity

Electrical conductivity

Mineral physics

Extremal bounds

Velocity–conductivity relationship

## ABSTRACT

Can mineral physics and mixing theories explain field observations of seismic velocity and electrical conductivity, and is there an advantage to combining seismological and electromagnetic techniques? These two questions are at the heart of this paper. Using phenomenologically-derived state equations for individual minerals coupled with multi-phase, Hashin–Shtrikman extremal-bound theory we derive the likely shear and compressional velocities and electrical conductivity at three depths, 100 km, 150 km and 200 km, beneath the central part of the Slave craton and beneath the Kimberley region of the Kaapvaal craton based on known petrologically-observed mineral abundances and magnesium numbers, combined with estimates of temperatures and pressures. We demonstrate that there are measurable differences between the physical properties of the two lithospheres for the upper depths, primarily due to the different ambient temperature, but that differences in velocity are negligibly small at 200 km. We also show that there is an advantage to combining seismic and electromagnetic data, given that conductivity is exponentially dependent on temperature whereas the shear and bulk moduli have only a linear dependence in cratonic lithospheric rocks. Focussing on a known discontinuity between harzburgite-dominated and lherzolitic mantle in the Slave craton at a depth of about 160 km, we demonstrate that the amplitude of compressional (P) wave to shear (S) wave conversions would be very weak, and so explanations for the seismological (receiver function) observations must either appeal to effects we have not considered, or imply that the laboratory data require further refinement.

© 2008 Elsevier B.V. All rights reserved.

## 1. Introduction

Petrological physical-property measurements in the laboratory connect geophysical observations to subsurface materials and processes. Most of the measurements are made on single grains of constituent minerals that form the lithosphere, and from those measurements equations are derived that best fit the data and show the dependence of various parameters, such as the bulk and shear moduli and electrical conductivity, on temperature, pressure, grain size, etc. Once those single grain equations are known, the next task is to determine the likely physical parameters of whole rocks using various mixing theories and relationships. Our approach here is to use extremal-bound theory for those mixing relationships, rather than the Voigt–Reuss–Hill (Voigt, 1928; Reuss, 1929; Hill, 1952) estimates more routinely applied in seismology.

We choose to be very selective in the type of rocks we wish to numerically manufacture, and restrict ourselves to dry, cratonic mantle which can be described in simple mineralogical and physical terms.

Although our selection suffers from not having the breadth of Hacker et al.'s (2003) consideration of the multitude of minerals in a subduction zone setting, we consider each mineral phase in great detail, and for both elastic moduli and electrical conductivity.

We construct typical continental lithospheric mantle “rocks” based on assemblages of four minerals, namely olivine, orthopyroxene, clinopyroxene and garnet, from known compositions at three depths, 100 km, 150 km and 200 km, below the Lac de Gras region of Slave craton (northern Canada) and below the Kimberley region of the Kaapvaal craton (South Africa). We choose these two regions as they are, by far, the best known geochemically and petrologically in the world. Furthermore, the two are clearly different in their chemical compositions (Stachel et al., 2003), and we wish to determine whether these chemical differences translate into measurable physical differences in velocity and conductivity. In particular, the central Slave craton displays a strong chemical stratification, with a high Mg# layer comprising 60% harzburgite (Hz) and 40% lherzolite (Lh) (Griffin et al., 1999; Menzies et al., 2004) to about 160 km (Menzies et al., 2004), overlying a more fertile, low Mg#, dominantly lherzolitic layer to a depth of around 200 km (Griffin et al., 1999; Menzies et al., 2004). In the upper layer 20–40% of the Hz is low-CaO Hz, evidence of the strong

\* Corresponding author.

E-mail addresses: [alan@cp.dias.ie](mailto:alan@cp.dias.ie) (A.G. Jones), [revans@whoi.edu](mailto:revans@whoi.edu) (R.L. Evans), [eatond@ucalgary.ca](mailto:eatond@ucalgary.ca) (D.W. Eaton).

depletion of this layer. In contrast, the Kimberley region of the Kaapvaal craton exhibits far more uniform properties without strong chemical layering, and with “normal” lherzolitic rocks throughout.

Our approach is similar to that of others, particularly Hacker et al. (2003), with their published Excel spreadsheet for a broader range of minerals (Hacker and Abers, 2004). We agree with the comment in Hacker et al. (2005) to Bosquet et al.’s (2005) criticism of their 2003 paper that this approach has the advantage that it is grounded in reality—known laboratory-determined petrophysical properties of minerals coupled with known mineral abundances and, in our case, a conservative mixing law that includes both grain and surface effects.

One important point in our analysis is that we exclude any “exotic” minor phases. These have less effect on seismic velocities, but some phases, such as carbon in graphite form or lining grain boundaries, have a considerable effect on electrical conductivity (e.g., Jones et al., 2003; Jones and Craven, 2004). Some support for the role of graphite in enhancing mantle conductivity comes from the depth extent of the Central Slave Mantle Conductor that appears to be limited to above the graphite–diamond stability field (Jones et al., 2003).

Kopylova et al. (2004) undertook a somewhat similar exercise for seismic velocities for the northern Slave and the southern Slave, but not for the central Slave which exhibits the strong petrological stratification. The mixing rule they adopted was a simple weighted arithmetic average of the velocities for the constituent minerals, rather than the formal extremal bound rules that we use here. Similarly, Bagdassarov et al. (2007) constructed electrical conductivity profiles from laboratory determinations of conductivity on minerals from xenoliths recovered on the Slave craton, but used a simple logarithmic averaging scheme for their mixing rule.

Having derived the velocities and conductivity at various depths beneath the Slave and Kaapvaal craton, we construct cross-plots to try to identify interdependence between the moduli (velocity) and conductivity. This is the reverse of the approach of Gibiansky and Torquato (1993, 1996) and Carcione et al. (2007) who defined formal relationships between moduli and conductivity for two-phase composites.

We consider separately the effects of varying each of the controlling conditions—temperature, iron content and other aspects of the chemical composition/mineralogy—and demonstrate that temperature has the greatest effect on the bulk physical properties.

Finally, we determine the parameters on either side of the harzburgite/lherzolite boundary at 160 km beneath the central part of the Slave craton. We demonstrate that, according to the best available mineral physics data and the most valid mixing theories, we should not be able to observe this boundary with teleseismic receiver functions, whereas one is clearly seen (Snyder et al., 2004). Thus we conclude that either the mineral physics data require refinement, and/or that there is an inadequately known scaling from the laboratory scale to the field scale, and/or that the mixing laws are inappropriate.

## 2. Seismic velocity of mantle minerals

### 2.1. Estimates of the bulk and shear moduli of mantle minerals

The bulk ( $K$ ) and shear ( $G$ ) moduli and density ( $\rho$ ) of the dominant mantle minerals olivine (Ol), orthopyroxene (Opx), clinopyroxene (Cpx) and garnet (Gt) have been measured by many laboratories over more than three decades, and Table 1 lists recently-reported values. For some of them the standard temperature and pressure (25 °C and 1 atm.) values are given, and there are noted variations of the moduli with pressure, temperature and magnesium number (Mg#,  $Mg/(Mg+Fe)$ ), usually multiplied by 100).

The variation of the moduli with pressure and temperature has also been reported by various laboratories, and example values are given in Table 1, some of which represent summaries themselves. There is clearly a wide range of reported values for the moduli, and their dependence on Mg#, temperature and pressure. For the purposes of our study, we take the formulae of James et al. (2004) for olivine, orthopyroxene and garnet, and the formulae of Goes et al. (2000) for clinopyroxene. Goes et al.’s (2000) formulations yield virtually the same moduli as those in Isaak et al. (2006) for an Mg# of around 90, but include the pressure dependence for the bulk modulus

**Table 1**

Values of bulk and shear moduli and density from various authors, with pressure, temperature and Mg# dependence where available

Mineral	$K_S$ (GPa)	$\delta K/\delta P$ ( $\delta K^2/\delta P^2$ )	$\delta K/\delta T$ (MPa/K)	$G$ (GPa)	$\delta G/\delta P$	$\delta G/\delta T$ (MPa/K)	$\rho$ (g/cm <sup>3</sup> )	Reference
Ol	–	–	–17.5	–	–	–13.7		I93
Ol	129.0	–	–16	82–30.0 $f$	–	–14	3.222	GGV00
Ol	129.0	–	–19	–	–	–	3.222	LL06
							+1.82 $f$	
Ol	<b>128.6</b>	<b>4.4</b>	<b>–18.2</b>	<b>79.1</b>	<b>1.71</b>	<b>–14.0</b>		<b>JBSBC04</b>
	<b>+7.0<math>f</math></b>	<b>–2.0<math>f</math></b>	<b>–0.09<math>f</math></b>	<b>–35.8<math>f</math></b>	<b>–1.23<math>f</math></b>	<b>–0.18<math>f</math></b>	+1.32 $f$	
Opx	102	10.9 (–1.6)	–	74.9	1.6	–	3.180	FLL98
Opx	111	–	–12	81	–	–11	3.198	GGV00
	–10.0 $f$	–	–	–29 $f$	–	–	–	
Opx	108.5	–	–26.3	77.9	–	–13.6	3.196	JSB07
Opx	102.5	–	–	74.2	–	–	–	PNSB07
Opx	114	–	–13	74	–	–11	3.204	LL07
							+0.799 $f$	
Opx	<b>106.5</b>	<b>11.0</b>	<b>–26.8</b>	<b>75.0</b>	<b>1.6</b>	<b>–12.0</b>		<b>JBSBC04</b>
	<b>–5.2<math>f</math></b>	<b>–2.56<math>f</math></b>						
Cpx	117.2	–	–	72.2	–	–	3.327	CB98
Cpx	<b>105</b>	–	<b>–13</b>	<b>67</b>	–	<b>–10</b>	3.280	<b>GGV00</b>
	<b>+13<math>f</math></b>			<b>–6<math>f</math></b>				
Cpx	116.5	–	–12.3	72.8	–	–9.98	–	IOL06
Cpx	117.6	6.4	–	–	–	–	–	NBTO05
Cpx	117	–	–15	67	–	–14	3.277	LL07
							+0.38 $f$	
Gt	154.5	4.71	–	89.7	4.71	–	–	JSSD04
Gt	173	–	–21	92	–	–10	–	GGV00
	+7 $f$	–	–	–7 $f$	–	–	–	
Gt	171	–	–16	91	–	–10	3.565	LL07
							+0.76 $f$	
Gt	<b>171.2</b>	<b>4.9</b>	<b>–19.8</b>	<b>93.0</b>	<b>1.56</b>	<b>–10.0</b>		<b>JBSBC04</b>

The boldfaced formulae are the ones adopted herein.

I93: Isaak (1993); CB98: Collins and Brown (1998); FLL98: Flesch et al. (1998); GGV00: Goes et al. (2000); IOL06: Isaak et al. (2006); JBSBC04: James et al. (2004); JSSD04: Jiang et al. (2004); NBTO05: Nestola et al. (2004); PNSB07: LL06: Liu and Li (2006); Perrillat et al. (2007); JSB07: Jackson et al. (2007);  $f$  = iron number ( $X_{Fe}$ ) =  $(Fe/(Fe+Mg)) = 1 - Mg\#/100$ .

derived by Nestola et al. (2004). The formulae we use for deriving the moduli and density are those in James et al. (2004), viz.,

$$\begin{aligned}(K_S)_{P,T} &= K_S + (\partial K_S / \partial P) \Delta P + (\partial K_S / \partial T) \Delta T, \\ G_{P,T} &= G + (\partial G / \partial P) \Delta P + (\partial G / \partial T) \Delta T \\ \rho &= \rho(1 - \alpha \Delta T + \Delta P / K_T).\end{aligned}$$

The assumptions implicit in our implementation of these formulae are discussed in James et al. (2004), and are:

- The  $P$ - $T$  derivatives are applicable over the whole range of pressures and temperatures of the lithospheric mantle, in our case from 3.00–6.3 GPa and 740–1250 °C respectively,
- Magnesium numbers for all four minerals are assumed equal, and,
- The elastic constants have no derivatives with regard to composition.

## 2.2. Conversion to velocities

We convert the shear and bulk moduli to seismic compressional ( $V_p$ ), shear ( $V_s$ ) and bulk ( $V_b$ ) velocities using the standard formulae

$$V_p = \sqrt{\frac{(\frac{4}{3}G + K_S)}{\rho}}, \quad V_s = \sqrt{\frac{G}{\rho}}, \quad \text{and} \quad V_b = \sqrt{\frac{K_S}{\rho}},$$

where  $\rho$  is the bulk density of the composite, given by

$$\rho = \sum_{i=1}^N x_i \rho_i,$$

and where  $x_i$  is the volume fraction of the  $i$ th phase of the  $N$ -phase medium. From these velocities and density we calculate  $P$ - and  $S$ -wave impedances given by the product of velocity and density, i.e., in terms of the moduli,

$$Z_p = \sqrt{\rho \left( \frac{4}{3}G + K_S \right)}, \quad \text{and} \quad Z_s = \sqrt{\rho G}.$$

From these impedances at an interface between two media one can define a reflection coefficient,  $R$ , given by the impedances in each of the media

$$R = \frac{Z_L - Z_U}{Z_L + Z_U},$$

where  $Z$  is the impedance in the upper (U) and lower (L) medium respectively.

## 2.3. Magnesium number variation

The iron content of the constituent minerals has a significant effect on the bulk and shear moduli, as one would expect intuitively. In the four minerals being considered, there is an Fe/Mg exchange, so that the ratio is given by the magnesium number (Mg#, see above). Some authors, (e.g., James et al., 2004), specify their results in terms of the Fe number, which is  $(1 - \text{Mg\#}/100)$ . Note that for bulk modulus, olivine and orthopyroxene behave differently with Mg#: olivine becomes less compressible with increasing iron content, whereas Opx becomes more compressible. However, the effects are small; for olivine the range is from 129.74 to 129.39 for Mg# from 88 to 93, whereas for Opx it is 105.88 to 106.14 respectively. For shear modulus, only olivine is reported to exhibit an Mg# sensitivity. It is large and positive varying from 74.80 to 76.59 for an Mg# range from 88 to 93. When converted into velocities however, these two variations are both overwhelmed by the density increase with increasing Fe content (decreasing Mg#), from 3.31 g/cm<sup>3</sup> to 3.38 g/cm<sup>3</sup> for Mg# varying from 93 to 88.

Chen et al. (1996) noted a strong  $V_p$  velocity increase with increasing Mg# for olivine, consistent with the results of James et al. (2004), when taking the density variation with Mg# into account (see

below). Kopylova et al. (2004) noted a decreasing  $V_p$  but increasing  $V_s$  with increasing Mg# of spinel and garnet peridotites. As the Slave lithospheric mantle is dominated by olivine (typically 80% or greater), these results based on direct measurements from xenoliths are difficult to reconcile with laboratory data for olivine.

Magnesium number variation with depth for the Slave craton are taken from Kopylova and Caro (2004, Fig. 13, Central Slave), and for the Kaapvaal craton from O'Reilly and Griffin (2006).

## 3. Electrical conductivity of mantle minerals

### 3.1. Brief review of temperature dependence of the conductivity of mantle minerals

Given its solid-state Arrhenius relationship, electrical conductivity of mantle minerals can be expressed as a summation of  $N$  thermally activated processes, viz.

$$\sigma = \sum_{i=1}^N \sigma_i e^{-E_i/kT},$$

where  $\sigma$  is the bulk conductivity, in Siemens/metre (S/m),  $k$  is Boltzmann's constant,  $\sigma_i$  is the zero temperature conductivity of phase  $i$ ,  $E_i$  is the activation energy of phase  $i$ ,  $T$  is the temperature in Kelvin, and subscript  $i$  refers to each of the processes. The majority of the minerals only have one derived activation energy reported, which is constant over the particular temperature range measured. Olivine differs in exhibiting more than one value over the temperature range of 720–1500 °C (Constable et al., 1992). The pre-exponential constant is usually given as a power of 10, i.e.,  $\sigma_0 = 10^x$ . In Table 2 we list the parameters best fitting experimental observations.

Olivine is the most-studied of mantle minerals. There was very poor agreement in the 1960s and early 1970s between different laboratories until there was appreciation of the need to do the laboratory experiments at appropriate oxygen fugacity ( $f_{O_2}$ ) conditions (Duba and Nicholls, 1973, highlighted in the excellent review paper by Duba, 1976). The effects of redox state, iron content, and electronic conduction at reducing conditions, all reviewed below, are also becoming better understood. Even so, there still is relatively weak agreement between various laboratories (see Table 3).

### 3.2. Oxygen fugacity dependence

Constable (2006), following the work of Constable and Roberts (1997), recently proposed a temperature–conductivity relationship for olivine that includes consideration of the redox state of the upper mantle under investigation. In his work, conductivity is given by the summation of two conduction mechanisms, one resulting from polarons (conducting electrons in an ionic crystal lattice) and the other from magnesium vacancies. The change in dominance of conduction mechanism between the two occurs at a temperature around 1300 °C (Schock et al., 1989), which is approximately the temperature at the base of the lithosphere. Conductivity can be thus described as

$$\sigma = \left[ \text{Fe}_{\text{Mg}}^{\bullet} \right] \mu_{\text{Fe}} e + 2 \left[ V_{\text{Mg}}'' \right] \mu_{\text{Mg}} e,$$

where the mobilities are given by,

$$\begin{aligned}\mu_{\text{Fe}} &= 12.2 \times 10^{-6} e^{-1.05(\text{eV})/kT}, \\ \mu_{\text{Mg}} &= 2.72 \times 10^{-6} e^{-1.09(\text{eV})/kT},\end{aligned}$$

and the concentrations by,

$$\begin{aligned}\left[ \text{Fe}_{\text{Mg}}^{\bullet} \right] &= b_{\text{Fe}}(T) + 3.33 \times 10^{24} e^{-0.02(\text{eV})/kT} f_{O_2}^{1/6}, \\ \left[ V_{\text{Mg}}'' \right] &= b_{\text{Mg}}(T) + 6.21 \times 10^{30} e^{-1.83(\text{eV})/kT} f_{O_2}^{1/6},\end{aligned}$$

**Table 2**  
Parameters for variation of electrical conductivity with temperature applicable to Mg#s in the range of 85–93

Mineral	$x_1$	$E_1$ (eV)	$x_2$	$E_2$ (eV)	Temperature range °C	Reference
Ol (Fo=91.7)	2.402	1.60	9.17	4.25	720–1500	CSD92
Ol	2.69	1.62	–	–	1200–1500	XPSR98
Ol (Fo=91.7)	2.50	1.5 (+PΔV term)	–	–	–	XSD00
Ol (Fo=89.1)	–1.185 (+fO <sub>2</sub> term)	0.531	–	–	1100–1300	DRIT05
Ol	(6.54–log(T))*f <sup>1.81</sup>	1.35	–	–	1150–1300	HSD93
Ol	–	–	–	–	–	C06
Ol Fo=100	2.77	0.984	–	–	522–970	HWC81
Ol Fo=90	1.54	0.777	–	–	593–939	HWC81
Ol Fo=80	7.76	0.683	–	–	527–939	HWC81
Opx	<b>3.72</b>	<b>1.80</b>	–	–	<b>1000–1400</b>	<b>XS99</b>
Cpx	<b>3.25</b>	<b>1.87</b>	–	–	<b>1000–1400</b>	<b>XSP00</b>
Gt	3.35	1.66	–	–	–	XSP00
Py100	2.67*	2.56*	–	–	1300–1700	RPKM06
Py100	4.26 <sup>c</sup>	2.40 <sup>c</sup>	–	–	–	this paper
Py85Alm15	2.42	1.50	–	–	1050–1550	RPKM06
Gt	<b>4.26 – 12.26f</b>	<b>2.40 – 6.0f</b>	–	–	–	<b>This paper</b>

The boldfaced formulae are the ones adopted herein.

C06: Constable (2006); CSD92: Constable et al. (1992); DRIT05: Du Frane et al. (2005); HSD93: Hirsch et al. (1993); HWC81: Hinze et al. (1981); RPKM06: Romano et al. (2006); XPSR98: Xu et al. (1998); XSD00: Xu et al. (2000a,b); XS99: Xu and Shankland (1999); XSP00: Xu et al. (2000b).

\*: These values from Romano et al. (2006) do not fit the data shown in their Fig. 2. <sup>c</sup>: Corrected values fitting data shown in Romano et al. (2006, Fig. 2).

f=iron number ( $X_{Fe}$ )=(Fe/(Fe+Mg))=1–Mg#/100.

where  $e$  is electron charge,  $T$  is temperature (in Kelvin), and  $k$  is Boltzman's constant. The unknowns in this equation are the two defect concentration terms,  $b_{Fe}$  and  $b_{Mg}$ , the temperature, and the oxygen fugacity. The former were estimated by Constable (2006) from the 3 data points in Du Frane et al. (2005), as

$$b_{Fe} = 5.06 \times 10^{24} e^{-0.357(eV)/kT}$$

$$b_{Mg} = 4.58 \times 10^{26} e^{-0.752(eV)/kT}$$

Temperature can be estimated from either geothermal models or from petrological analyses of mantle xenoliths. This is discussed further below.

Oxygen fugacity can also be estimated from petrological analyses of mantle xenoliths. Note that the conductivity–temperature curves derived by Constable (2006) assume a single mantle oxygen fugacity, either QFM (quartz–fayalite–magnetite) oxygen buffered or IW (iron–wüstite) buffered. Constable (pers. comm., 2007) used the following for estimates of QFM and IW oxygen fugacity:

$$\text{QFM } \log(fO_2 \text{ Pa}) = -29.458/T + 16.9815,$$

$$\text{IW } \log(fO_2 \text{ Pa}) = -27.217/T + 11.5733,$$

where  $T$  is the temperature in Kelvin. These values differ from the widely used ones of Myers and Eugster (1983), which are

$$\text{QFM } \log(fO_2 \text{ atm}) = -24.441.9/T + 8.290,$$

$$\text{IW } \log(fO_2 \text{ atm}) = -26.834.7/T + 6.471.$$

Converting to pressure in Pa using the standard value of 1 atm=101.325 kPa, yields, for the QFM buffer,

$$\text{QFM } \log(fO_2 \text{ Pa}) = -24.441.9/T + 13.296.$$

Constable's formulation results in more reduced pressures at low temperatures (below 1100 °C), and more oxidizing pressures at high temperatures. Log( $fO_2$ ) for QFM buffer at 645 °C from Constable's formula is –15.11, whereas for Myers and Eugster's it is –13.33. At 1250 °C the two yield –2.36 and –2.75 respectively. Herein we adopt the formulation of Myers and Eugster (1983), given above, as that is the more commonly accepted one.

Du Frane et al. (2005) also considered a description of conductivity of olivine that took into account the redox state of the mantle, but in their case they included the contribution from electronic conduction at reducing conditions (Stockler, 1978). Their geometrical mean result

for their data (they considered anisotropy) derived at temperatures of 1100, 1200 and 1300 °C, fit the equation

$$\sigma = [2.51f_{O_2}^{2/11} + 0.0653] e^{-0.531(eV)/kT} \quad (\text{S/m}),$$

and their equation is tabulated for pertinent temperatures and oxygen fugacities in Table 3. Note that their results suggest far higher electrical conductivity for the upper mantle lithosphere than proposed by the SO2 (Constable et al., 1992) and SEO3 (Constable, 2006) models. However, in the temperature range of their data, the agreement with all other models is better than 0.5 log units (Table 3).

McCammion and Kopylova (2004) noted the added complication that oxygen fugacity decreases with increasing depth, from approx. –2 Δlog( $fO_2$ ) at 100 km to –4 Δlog( $fO_2$ ) at 200 km, relative to QFM buffer, in the Slave lithospheric mantle, and these values are also appropriate for the Kaapvaal cratonic mantle (Woodland and Koch, 2003). However, this variation of  $fO_2$  with depth is barely significant in terms of the electrical conductivity of the cratonic lithosphere: a constant  $fO_2$  of say –2 Δlog( $fO_2$ ) cf. QFM would result in a log (conductivity) of –3.05 at a temperature of 1250 °C (temperature at 200 km beneath the Kaapvaal craton), whereas an  $fO_2$  of –4 Δlog( $fO_2$ ), which is in fact more reducing than the IW buffer, results in a log (conductivity) of –3.15. Indeed, ignoring  $fO_2$  completely and using model SO2 of Constable et al. (1992), Table 2, yields a log(conductivity) of –2.88.

### 3.3. Magnesium number variation

Decreasing Mg# by replacing magnesium by iron results in increased electrical conductivity in all minerals, especially olivine

**Table 3**  
Logarithm (electrical conductivity) of olivine from different models at relevant temperatures, Mg#s, and oxygen fugacities of interest (see Table 6)

Temperature (°C)	Log ( $fO_2$ ) (Pa)	Mg#	SO2 (CSD92)	Xu (XPSR98)	Hirsch (HSD93) (Mg#)	SEO3 (C06) ( $fO_2$ )	DuFrane (DRIT05) ( $fO_2$ )
645	–13.3	93.5	–6.38	–6.20	–5.98	–6.66	–4.10
740	–10.8	92.3	–5.56	–5.37	–5.20	–5.89	–3.83
875	–8.00	92.0	–4.62	–4.42	–4.43	–4.99	–3.51
1010	–5.75	91.0	–3.88	–3.67	–3.76	–4.26	–3.26
1125	–4.19	90.2	–3.37	–3.15	–3.30	–3.74	–3.09
1250	–2.75	89.0	–2.89	–2.67	–2.85	–3.25	–2.93

(e.g., Schock et al., 1989; Vacher and Verhoeven, 2007). This well-known effect, where iron chemically substitutes for magnesium in the dodecahedral site while maintaining a fixed lattice symmetry, has been studied in olivine and pyroxene since the early 1980s (Hinze et al., 1981; Seifert et al., 1982), and most recently in garnet by Romano et al. (2006). At temperature and  $fO_2$  conditions of the cratonic lithospheric mantle, even minor amounts of Fe, e.g., comparing pure fosterite with  $FO_{99.99}$ , have been shown to affect material properties (Hirsch and Shankland, 1993). However, the number of lab studies is few. For our purposes the results of Hinze et al. (1981), Hirsch et al. (1993) and Romano et al. (2006) are the most pertinent. Olivine ranges from forsterite (Mg# of 100) to fayalite (Mg# of 0), and garnet ranges from pyrope (Mg# of 100) to almandine (Mg# of 0). For our purposes we consider Mg#s in the range of 88 to 93, which are those observed in the mantle lithospheres of the Slave and Kaapvaal cratons.

Most of the work on olivine by U.S. laboratories has been conducted on single crystals of San Carlos olivine, which has an Mg# of around 91.7, i.e., in the middle of the range of interest. Hinze et al. (1981) studied synthetic olivine from fayalite to forsterite composition. Listed in Table 2 are the conductivity values of Hinze et al. (1981) for Mg#s of 100, 90 and 80 for an Fe-buffered system, which is closer to the oxygen fugacity ( $fO_2$ ) of Archean lithospheric mantle (Ballhaus, 1993; McCammon and Kopylova, 2004).

Hirsch et al. (1993) conducted similar experiments with grown crystals of Mg# 66.5, 81.65 and 88.9, and with San Carlos olivine (their sample had an Mg# of 91.35). Their observations were fit by the equation

$$\sigma = \left( \frac{10^{6.54}}{T} \right) X_{Fe}^{1.81} e^{-1.35(eV)/kT},$$

where  $X_{Fe}$  is the iron number.

This formulation suggests a conductivity contrast of 0.16 log units at the transition from the depleted harzburgitic region (Mg#=92.0) to the less-depleted, more iron rich, lherzolitic region (Mg#=90.2) in the mid-lithosphere beneath the central part of the Slave craton (see below). This change is far greater than any change that might be due to oxygen fugacity or to compositional variation.

Important to note in Hirsch et al.'s (1993) work is their observation that their heterogeneous samples showed an even greater Fe-dependence: the exponent on the  $X_{Fe}$  component was 1.85 rather than 1.81 for their homogeneous samples.

For garnet there is also a strong dependence on magnesium number. Romano et al. (2006) studied garnet over the full compositional range from pyrope (100% Mg) to almandine (100% iron). Below we list the parameters for Mg# of 60, 85 and 100, given by Romano et al. (2006). We take the experimental values for Py85Alm15 for our lherzolitic garnet calculations, and linearly interpolate between Py100 and Py85Alm15 to estimate the parameters for an ultra-depleted harzburgitic garnet with an Mg# of 92 ( $x_1=2.54$  and  $A_1=1.99$ ). Romano et al.'s (2006) data for the two pyrope-almandine garnets Py100 (H1741, Mg# of 100) and Py85Alm15 (H1836, Mg# of 85) at 10 GPa are the most pertinent of their studies. Romano et al. (2006) give the pre-exponent constant ( $\sigma_0$ ) and activation energy values listed in Table 2 for these garnets, of (466  $\Omega$  m, 2.56) and (262  $\Omega$  m, 1.50) respectively. However, the values listed in Table 2 for the Py100 sample do not fit their data shown in their Figs. 2 or 3. Reading their values off Fig. 2 and performing a regression shows that the data are fit with a  $\sigma_0$  and activation energy of (18,280  $\Omega$  m, 2.40) respectively. For the purposes of this paper, we adopt an  $X_{Fe}$  dependent Gt conductivity as highlighted in Table 2.

Laboratory studies of the variation of iron content on pyroxenes are lacking. There is not a single study of clinopyroxene, and only one study, which dates from quarter of a century ago, on orthopyroxene (Seifert et al., 1982). The results of Seifert et al. (1982, reviewed in Vacher and Verhoeven, 2007) are intriguing, to say the least, as their

data fit a formulation with a negative exponent of  $-1.28$  on  $X_{Fe}$ , i.e., a decreasing conductivity with increasing iron content. In the absence of data for clinopyroxene, Vacher and Verhoeven (2007) adopt the same negative exponent for it as for orthopyroxene. In our case, given the absence of data, we choose the more conservative approach of assuming that the exponent is zero, i.e., that there is no variation of conductivity with iron content for the pyroxenes.

### 3.4. Pressure effects

Pressure effects on the conductivity of mantle minerals have been studied by a number of authors, and are generally thought to be negligibly small when compared to temperature effects (e.g., Shankland et al., 1993; Xu et al., 2000a; Nover, 2005). Recently though, Katsura et al. (2007) studied enstatite (Opx), with a composition of (Mg<sub>0.93</sub>Fe<sub>0.07</sub>)SiO<sub>3</sub>, at lower-mantle pressures and their samples exhibited strong pressure dependence of over an order-of-magnitude increase in conductivity with pressure increase from 25 GPa to 35 GPa. Romano et al. (2006) also reported a strong pressure dependence on Gt with pressure increasing from 10 GPa to 19 GPa. These high pressures are not appropriate for our study of lithospheric minerals, and we assume that pressure dependence is negligible.

### 3.5. Effect of hydrous minerals

Karato (1990) suggested that hydrogen diffusion could be a significant contributor to electrical conductivity of normally anhydrous mantle minerals like olivine, and that indeed geophysical remote sensing methods could be used to determine the hydrogen distribution (Gaillard et al., 2003; Karato, 2006). Laboratory measurements testing this model though are not conclusive. Poe et al. (2005) essentially confirms Karato's (1990) suggestion, but require concentrations of several hundred ppm in olivine. Wang et al. (2006) show data that argue for a modified form of Karato's (1990) original model to explain enhanced conduction in wet samples. Yoshino et al. (2006) see lower (but still enhanced relative to dry compositions) conductivities than Wang et al. (2006) at given water content. They do not see any evidence for enhanced conductivity along the  $a$ -axis, something that Karato's model of hydrogen enhanced conductivity predicts based on observations that the diffusion of hydrogen in olivine is significantly faster in this direction (Kohlstedt and Mackwell, 1998).

Hirth et al. (2000) showed that long period, single station data in the Archean Superior Province are consistent with a dry lithospheric mantle between about 150 km and 250 km depth. However, the presence of water cannot be ruled out if the mantle is isotropic. Hirth et al. (2000) favoured a dry composition as observed seismic anisotropy suggests  $a$ -axis alignment of olivine which, in turn, would predict anisotropic electrical conductivity, something that was not apparent beneath the study area in the Superior Province. Other areas of the Superior Province have been known for over a decade to exhibit high degrees of electrical anisotropy (Mareschal et al., 1995; Ferguson et al., 2005; Frederiksen et al., 2006), although in at least one of these instances the anisotropy was inferred to be due to a graphite distribution resulting from internal deformation within the cratonic lithosphere.

Beran and Libowitzky (2006) and Grant et al. (2007) note that the water content stored in olivine and mantle garnet is very low compared to that in pyroxenes, and Wang et al. (2006) infer that the water content in the continental lithospheric upper mantle is  $<10^{-3}$  wt.%. The values in Grant et al. (2007) are surprising, in that the water content appears to be relatively independent of the age of the lithosphere studied. Clinopyroxene exhibits the highest contents, around 400 ppm, followed by orthopyroxene at around 200 ppm. Olivine is below 55 ppm, and generally in the low tens of ppm, whereas there is virtually no water in garnet. In addition, if Karato's model is correct, then the water content is only important for conductivity if the diffusivity of hydrogen is fast in the

mineral of interest. There is not a lot of reported data on pyroxenes, but what there is, reviewed in [Ingrin and Blanchard \(2006\)](#), suggests that the addition of water to Opx would not enhance conductivity. [Mierdel et al. \(2007\)](#) show that aluminous Opx can hold large quantities of water under lithospheric mantle conditions, yet the diffusivity data would not suggest that such a mineral would be electrically conductive.

Given that the regions we are studying are depleted (no hydrous minerals), are virtually Cpx free, that olivine and Opx dominate and the maximum water content in olivine is well below 50 ppm and there is slow diffusivity in Opx, the effect of hydrogen diffusion can thus be neglected.

### 3.6. Effect of anisotropy

The conductivity of dry olivine shows at most a factor of ~2–3 anisotropy, with the *a*- and *b*-axes having almost identical conductivities, and the *c*-axis having the higher conductivity values ([Constable et al., 1992](#); [Xu et al., 2000b](#); [Du Frane et al., 2005](#)). Thus, for mantle rocks with a strong alignment of olivine *a*-axis, the conductivity under dry conditions is not expected to show significant anisotropy. However, as discussed in the previous section, it has been argued that the presence of water in olivine should enhance bulk mantle conductivity, particularly under anisotropic conditions ([Karato, 1990](#)). Other mantle phases are not expected to contribute to electrical anisotropy, even under hydrous conditions.

The amounts of electrical anisotropy possible due to hydrogen have been estimated to be only a factor of 3–4 ([Simpson, 2002](#); [Simpson and Tomassi, 2005](#)), based on calculations including reasonable estimates of shear strain and allowing for the mixing effects of the conductivities in other crystallographic directions. [Evans et al. \(2005\)](#) saw a factor of ~4 in anisotropy of the upper mantle in the oceanic lithospheric mantle east of the East Pacific Rise, and this is roughly consistent with the anisotropy predicted by [Simpson \(2002\)](#) for about 50% alignment of olivine *a*-axis. However, the amount of water expected to be present in continental lithospheric mantle is much less than in oceanic lithosphere, and so [Simpson and Tomassi \(2005\)](#) argue that evidence of electrical anisotropy in the continents suggests that other mechanisms, perhaps at grain boundaries, are important contributors to bulk conductivity.

As mentioned above, laboratory measurements on the impact of water on conductivity, and particularly whether hydrogen diffusion can cause significant electrical anisotropy, remain controversial.

### 3.7. Effect of grain size

Recently, [ten Grotenhuis et al. \(2004\)](#) observed an increasing conductivity with decreasing grain size in fine grained forsterite (Mg# = 100), suggesting that surface conduction may be an important contribution to the total conductivity of a rock. They proposed a model in which the bulk conductivity  $\sigma$  is given by the summation of the grain boundary conductivity  $\sigma_{gb}$  and the grain interior conductivity  $\sigma_{gi}$ , given as a function of the grain boundary width  $\delta$  divided by the grain size  $d$ , viz.,

$$\sigma = \sigma_{gi} + \sigma_{gb} \left[ 1 - \left( 1 - \frac{3\delta}{d} \right)^{2/3} \right].$$

With typical values of  $\delta$  of 1 nm ([Farver et al., 1994](#)), grain-boundary conduction dominates for grains smaller than about 1 nm, and grain-interior conduction dominates for larger grains. Others have proposed that the appropriate circuit is a series one, not a parallel one, so that it is the reciprocals that must be summed (e.g., [Yi et al., 2005](#)).

This observation remains controversial, however, as other workers have measured conductivities on single crystals and samples with a range of grain sizes and have not seen any systematic variation in conductivity with grain size ([Roberts and Tyburczy, 1991](#); [Xu et al.,](#)

[2000b](#); [Wang et al., 2006](#)). The grain sizes used by [ten Grotenhuis et al. \(2004\)](#) are very small (a few microns) and, while possibly applicable to shear zones and areas of high deformation, are not applicable to cratonic lithospheric mantle in general where xenoliths commonly reveal coarse textures with grain sizes on the order of 1 cm (e.g., [Finnerty and Boyd, 1987](#)). In addition, [Yi et al. \(2005\)](#) analysed grain interior and grain boundary conduction in pyroxenes, and found that grain-boundary conduction is important at high frequencies, above 100 Hz.

In our case, we consider the grains in the cratonic lithosphere to be typically 1 cm in size, and the frequencies penetrating below 40+ km are of the order of 0.1 Hz and lower, thus generally we can ignore the effect due to conduction by grain boundaries. We do, however, incorporate consideration of such an effect in our extremal bound derivations below.

### 3.8. Controls on electrical conductivity: Summary

Given the various factors that can affect electrical conductivity of lithospheric mantle minerals, as we show below the strongest is temperature, followed by iron content. Variation in Mg#, even by a small amount, is significantly more important than consideration of oxygen fugacity. Conductivity is expressed directly as a function of  $X_{Fe}$  to the power 1.81 or greater ([Hirsch et al., 1993](#)), whereas it goes as a function of  $fO_2$  to the power 1/6th ([Constable, 2006](#)) or 2/11th ([Du Frane et al., 2005](#)). At a temperature of 1000 °C, changing from an Mg# of 93.5 to 89 increases conductivity by a factor of over 2.5 ( $\log(\sigma)$  from -4.06 to -3.64 using [Hirsch et al., 1993](#)), whereas decreasing  $fO_2$  by 2 log units from -2 to -4 (c.f. QFM buffer), decreases conductivity by a factor of only 3% ( $\log(\sigma)$  from -4.305 to -4.317, using [Constable, 2006](#)). However, an increase in conductivity by a factor of 2.5 can be accomplished by increasing temperature by less than 100 °C (from 1000 °C to 1090 °C).

Olivine and garnet have been studied, and we have formulations for them. Unfortunately, laboratory measurements on the variation of conductivity with iron content for pyroxenes are lacking, and the only study conducted ([Seifert et al., 1982](#); reviewed in [Vacher and Verhoeven, 2007](#)) yields a suspicious result of decreasing conductivity with increasing iron content. [Vacher and Verhoeven \(2007\)](#) extend this result for orthopyroxene to both clinopyroxene and, oddly, to garnet. Observations by [Romano et al. \(2006\)](#) demonstrate that certainly the latter is an incorrect assumption. In the absence of conclusive data, we assume that varying iron content over the small range of Mg# of 93.5 to 89 has a negligible effect on the conductivity of pyroxenes.

The four equations we use for conductivity, as a function of temperature ( $T$ ) and iron content ( $X_{Fe}$ ), are thus

$$\begin{aligned} \sigma_{Ol} &= \left( \frac{10^{6.54}}{T} \right) X_{Fe}^{1.81} e^{-1.35(eV)/kT}, \\ \sigma_{Opx} &= 10^{3.72} e^{-1.80(eV)/kT}, \\ \sigma_{Cpx} &= 10^{3.25} e^{-1.87(eV)/kT}, \quad \text{and,} \\ \sigma_{Gt} &= 10^{(4.26-12.26X_{Fe})} e^{-(2.40-6.0X_{Fe})(eV)/kT}. \end{aligned}$$

## 4. Cratonic geotherms

In order to derive the moduli and electrical conductivity, we require knowledge of temperature beneath the regions of interest. Using published cratonic geotherms, we assign temperatures of 740, 1010, and 1250 °C and 645, 875, and 1125 °C at depths of 100 km, 150 km and 200 km for the Kaapvaal and central Slave (Lac de Gras region) cratons respectively, based on the thermal arguments of [Jones \(1988\)](#) and [Mareschal et al. \(2004\)](#). The difference between the two is not surprising since the Kaapvaal craton is known to have higher heat flow across the Moho than other Archean cratons (e.g., [Jaupart and Mareschal, 1999](#)).

We note that the geotherm of Mareschal et al. (2004), based on heat flow and thermal modelling, is some 50–100 °C cooler than the petrologically-defined geotherm predicted on the basis of xenoliths from a kimberlite pipe (Jericho) in the northern Slave craton (Russell and Kopylova, 1999). The same is true of the Kaapvaal craton, with petrologically–geochemically defined estimates (e.g., Kronrod and Kuslov, 2007) of 815, 1000, and 1225 °C being generally higher than those defined from thermal arguments by Jones (1988). One must be careful of avoiding a circular argument; we should not take a geotherm defined on the basis of seismology and petrology (e.g., Kronrod and Kuslov, 2007) in order to obtain a temperature from which we ultimately derive a velocity! We wish to ensure independence, so adopt the temperatures given by modelling of heat flow data.

## 5. Density estimates of mantle minerals

In order to calculate physical properties in the mantle we need to know the density of mantle minerals, and the variation of density with depth. Density estimates are given in Lee (2003), as listed in Table 4, together with those used by Goes et al. (2000) for the whole of the lithosphere. (Note that there is an error in column labelling in Table 1a of Lee (2003); for the spinel peridotites the columns are OPX, CPX, OL and SPI, not OPX, CPX, GT and OL, which are correct for the garnet peridotites.)

The results of Lee (2003) are surprising, as one would expect the higher pressure mineral phases, as expressed in garnet peridotite, to exhibit higher densities than the lower pressure phases in spinel peridotite. Density increase with depth is exhibited in the data of Kelly et al. (2003), from a suite of xenoliths from the Kaapvaal craton discussed in Boyd et al. (1999), going from low-T spinel (<100 km) to low-T garnet (100–180 km) to high-T garnet (>180 km) peridotites. The formulae of James et al. (2004), which are very close to those of Li and Liebermann (2007), are also questionable as they are not pressure dependent. However, Mg# generally decreases with depth, which will result in density increase through increased iron content. The dominant constituent of lithospheric rocks is olivine, and using Li and Liebermann's (2007) formula of  $\rho = 3.222 + 1.182 X_{\text{Fe}}$  its density increases from 3.305 g/cm<sup>3</sup> to 3.364 g/cm<sup>3</sup> for Mg# decrease from 93 to 88, which approaches the density increase observed (see below). In view of these considerations we take Li and Liebermann's (2007) formulae for calculating the individual densities of the minerals.

However, as our main use of density is to convert from bulk and shear moduli to seismic velocity, and to calculate the pressure at given depths, for the Kaapvaal craton we adopt the (visual) average density of the data shown in Fig. 2 of Kelly et al. (2003) of 3.31 g/cm<sup>3</sup> at 100 km, 3.36 g/cm<sup>3</sup> at 150 km, and 3.38 g/cm<sup>3</sup> at 200 km (calculated using the observed mode and mineral compositions). These values are somewhat higher than the averaged values of Kuskov et al. (2006) of 3.279, 3.327 and 3.361 g/cm<sup>3</sup> at those same depths. For the central Slave craton we use values of 3.28 g/cm<sup>3</sup> (Kopylova et al., 2004), 3.37 g/cm<sup>3</sup> (O'Reilly and Griffin, 2006) and 3.45 g/cm<sup>3</sup> (O'Reilly and Griffin, 2006) respectively. These values are less than the average Archean density values given in Poudjom Djomani et al. (2001, Fig. 6) at those

depths of 3.331, 3.342 and 3.352 g/cm<sup>3</sup>. They convert to Mg#s of 93.2, 89.4 and 87.9 for the Kaapvaal craton, and 95.4, 88.6, and 82.6 for the Slave craton using James et al.'s (2004) formula, which are inconsistent with those observed; 92.3, 91.0 and 89.0 (O'Reilly and Griffin, 2006) for the Kaapvaal craton, and 93.5, 92.0 and 90.2 (O'Reilly and Griffin, 2006) for the central Slave craton.

The averaged density stratification for the Kaapvaal craton is thus 2.7 g/cm<sup>3</sup> to 40 km, 3.30 g/cm<sup>3</sup> to 100 km, 3.335 g/cm<sup>3</sup> to 150 km, and 3.37 g/cm<sup>3</sup> to 200 km, and for the Slave craton is 2.7, 3.280, 3.325 and 3.39 g/cm<sup>3</sup>, which yields almost the same lithostatic pressures at all three depths beneath both cratons, despite their different density–depth profiles.

## 6. Physical parameters of mantle assemblages using mixing and effective medium theories

### 6.1. Voigt–Reuss–Hill and geometric mean formulations

The bulk (*K*) and shear (*G*) moduli of a composite medium has commonly been derived using the well-known Voigt (1928) or Reuss (1929) estimates. The Voigt estimate assumes equal strain in both phases of a two-phase system, and the Reuss estimate assumes equal stress. Essentially, the Voigt estimate assumes that the inclusions are rigid, whereas the Reuss estimate assumes that the inclusions are voids (e.g., Li and Wang, 2005). These two estimates lead to bounds that lie relatively far apart, leading researchers to propose other estimates. The most common in use is the arithmetic average of the Voigt and Reuss estimates, the so-called Voigt–Reuss–Hill (1952) estimate, VRH. Recently, Ji et al. (2004) suggested, based on empirical observations, that the geometric mean of the Voigt and Reuss estimates provides a superior estimate, called herein the Voigt–Reuss–Ji (VRJ) estimate.

### 6.2. Hashin–Shtrikman extremal bounds

Bounds that give the most extreme values that can be possibly obtained offer the advantage that they yield the most conservative yet physically-realizable range possible for the particular physical parameter under consideration, without assuming perfectly compressible or perfectly incompressible inclusions. The extremal bounds of mixing two phases were first developed by Maxwell–Garnet (1904) for treating mixtures of two coloured glasses. In a series of papers in the early 1960s Hashin and Shtrikman (1962a,b, 1963) developed the same concepts for extremal bounds as Maxwell–Garnet (1904) for mixing two phases. Hashin–Shtrikman (HS) bounds have found application in many fields of science. For electrical conductivity, the lower bound is given by assuming non-interconnected conductive inclusions in a resistive matrix, whereas the upper bound is given by assuming non-interconnected resistive inclusions in a conductive matrix. Similarly, in seismology the bounds are exact results of composite sphere assemblages (Hashin, 1970; Watt et al., 1976).

Berryman (1995) extended these bounds for multiphase materials, focussing particularly on electrical conductivity ( $\sigma$ ) and the bulk (*k*) and shear (*G*) moduli. His formulae are:

$$\sigma_{\text{HS}}^- = \left( \sum_{i=1}^N \frac{x_i}{\sigma_i + 2\sigma_{\text{min}}} \right)^{-1} - 2\sigma_{\text{min}},$$

$$K_{\text{HS}}^- = \left( \sum_{i=1}^N \frac{x_i}{K_i + \frac{4}{3}K_{\text{min}}} \right)^{-1} - \frac{4}{3}K_{\text{min}}, \quad \text{and}$$

$$G_{\text{HS}}^- = \left( \sum_{i=1}^N \frac{x_i}{G_i + G_{\text{min}}} \right)^{-1} - G_{\text{min}},$$

where superscript “–” denotes the lower bound and  $x_i$  denotes the volume fraction of the *i*th component. The upper bounds are given by

**Table 4**  
Density values of mantle minerals

Rock type	Ol	Opx	Cpx	Gt	Reference
Spinel peridotite	3.349	3.294	3.318	–	L03
Garnet peridotite	3.332	3.267	3.300	3.713	L03
Average	3.222	3.198	3.280	3.565	GGV00
Average	3.22 + 1.32 <i>f</i>	3.21 + 0.80 <i>f</i>	3.280	3.710	JBSBC04
Average	3.222 + 1.182 <i>f</i>	3.204 + 0.799 <i>f</i>	3.277 + .38 <i>f</i>	3.565 + 0.76 <i>f</i>	LL07

L03: Lee (2003); GGV00: Goes et al. (2000); JBSBC04: James et al. (2004); LL07: Li and Liebermann (2007);  $f = X_{\text{Fe}} = (\text{Fe}/(\text{Fe} + \text{Mg})) = 1 - \text{Mg}\#/100$ .

**Table 5**  
Modal mineralogies for the Kaapvaal and Slave cratons

Craton	OI	Opx	Cpx	Gt	Mg#	Reference
Kaapvaal average	65	24	4	7	92.3	G99
Kaapvaal average	65.5	26.9	6.1	1.3	92.0	KKA06
Slave average	79	13	2	6	91.9	G99
Slave Hz region (to 160 km)	75	23	0	2	93.5	G07
Slave Lh region	73	20	3	4	90.2	G07
Northern Slave upp.lith.	72	26	7	7	92.9	KR00
Northern Slave low.lith.	69	19	1.5	0	91.8	KR00

G99: Griffin et al. (1999); KR00: Kopylova and Russell (2000); KKA06: Kuskov et al. (2006); G07: Grütter (pers. comm., 2007).

the same formulae, substituting the maximum values,  $\sigma_{\max}$ ,  $K_{\max}$  and  $G_{\max}$ , for the minimum ones. The Hashin–Shtrikman bounds for moduli were compared to the Voigt–Reuss–Hill bounds by Watt et al. (1976), and the superiority of the former over the latter is unequivocally established. In particular, even for single crystal composites the VRH average for many materials lie outside the HS bounds, thus are unreliable (Watt et al., 1976).

Despite Watt et al.'s (1976) remarks, there are few studies that utilize multi-phase Hashin–Shtrikman bounds in seismology for deriving the moduli of composite materials. Notable exceptions are the papers by Vacher et al. (1996), Cammarano et al. (2003), Hacker et al. (2003), and Schutt and Leshner (2005). Recently Li and Wang (2005) proposed tighter bounds for two-phase composites than those from Hashin–Shtrikman theory; however, we prefer a more conservative approach in this analysis. Rigorous bounds for the bulk and shear moduli have been developed for two-phase mixtures in three dimensions by Gibiansky and Milton (1993) and Milton and Berryman (1997), and those authors show that the rigorous bounds reduce precisely to the Hashin–Shtrikman ones when all the constituent moduli are real. Whether the bounds above hold rigorously in the multi-phase case is yet to be demonstrated.

Two-phase Hashin–Shtrikman bounds have been applied routinely in electrical conductivity studies. Multi-phase HS studies have been conducted by Park and Ducea (2003) and Ledo and Jones (2005); the latter used the conductivity mixing formula for 3-phase assemblages of olivine, Opx and Cpx for a region in northern British Columbia/southern Yukon, Canada, to determine the maximum permitted temperature of the lithospheric mantle region where a seismic velocity anomaly was ascribed to elevated temperatures. Ledo and Jones (2005) demonstrated that such a temperature anomaly was not permissible according to the conductivity data.

Tighter bounds than the Hashin–Shtrikman ones can be derived if one assumes a different inclusion shape, such as needles, thin disks or penny-shaped cracks rather than spheres (e.g., Watt et al., 1976; Berryman, 2006). However, spheres lead to the broadest bounds possible, and so is the most conservative assumption one can make.

Having said that, a recent paper by Salje (2007) discusses possible explanations for observations of elastic properties that lie outside the Hashin–Shtrikman bounds, e.g., Ji and Wang's (1999) studies of forsterite–enstatite composites, arguing that the scaling of the volume proportions in mineral assemblages is not truly represented by the nominal volume proportion  $x$  of each phase. Salje (2007) suggests that interfacial effects scale with  $x(1-x)$  and that, in the case of certain

assemblages, the scaling is entirely with  $x^2$  rather than  $x$ . A more realistic scaling replaces  $x$  in the relevant averaging schemes by  $x(1-S)+Sx^2$  where surface parameter  $S$  lies in the range of 0–1 and weights the effect of the non-linearities in the volume expansion of the averaging schemes.  $S$  is expected to be grain-size dependent. A value of  $S=1$ , i.e., replacing  $x$  with  $x^2$  in the Hashin–Shtrikman bounds formulae above, was argued by Salje (2007) to explain Ji and Wang's (1999) anomalous data completely.

We explore the effects of including interface and surface effects by replacing  $x$  with  $x(1-S)+Sx^2$  in the above Hashin–Shtrikman bounds formulae, and determining the bounds for  $S=0$  (no surface effects) and  $S=1$  (only surface effects). However, as we show, the effects are minor. We do not explore composites made of dissimilar sizes grains nor do we explore non-linear effects, either of which could be highly important.

Recently Afonso et al. (2005) extended the 2-phase shear-lag mixing model of Cox (1952) to 3-phases, and proposed that it provides a superior estimate than either the VRH/VRJ or HS estimates. They showed in particular that both the VRH and VRJ estimates for Young's modulus poorly describe laboratory observations for 2-phase composites (Fig. 3, Afonso et al., 2005). They do not elaborate why their estimates are superior to the HS ones, but as they only treat 3-phase composites we cannot adopt their approach herein.

## 7. Application to the Slave and Kaapvaal cratons

We wish to apply the above-defined HS formulae to assemblages of rocks from the cratonic lithospheric mantle in order to test whether there should be an observable difference in physical properties within and between cratons. We take as our example lithospheres representative modal mineralogies from the two geochemically and petrologically best-known cratons, namely the Kaapvaal craton in South Africa and the Slave craton in northern Canada. In Table 5 we list the average modal mineralogies for the two cratons, from Griffin et al. (1999).

In the case of the Slave craton we define two assemblages, one for the known ultra-depleted, harzburgitic G10 region in the upper mantle (to about 160 km) of the central Slave craton beneath the Lac des Gras kimberlite field (Griffin et al., 1999; Grütter et al., 1999), and the second for the deeper lherzolitic G9 region (Griffin et al., 1999; Menzies et al., 2004). This is to examine the variation beneath the Slave craton, and we test whether the differences between the upper and lower lithosphere in the central Slave can be modelled with our composite assemblages.

We calculate the mineral bulk and shear moduli and electrical conductivity at three depths, 100 km, 150 km and 200 km (Table 7). The first is in the middle of the lithosphere. The second is at approximately the graphite–diamond stability field boundary, and at the base of the central Slave's ultra-depleted layer, and the third is close to the base of the lithosphere. For these, we need the other parameters discussed above and listed in Table 5.

The calculations of the moduli, with derived velocities and conductivity are given in Table 6 for all three depths for both cratons for the minerals considered. From these values, we compute the bulk rock properties using Hashin–Shtrikman lower (HS<sup>-</sup>) and upper (HS<sup>+</sup>) bounds, and for both grain ( $S=0$ ) and grain boundary ( $S=1$ ) effects.

**Table 6**  
Parameters at depths of 100, 150 and 200 km beneath the Kaapvaal and Slave cratons and assumed modal mineralogies

Craton	Depth (km)	Density (g/cm <sup>3</sup> )	Temperature (°C)	Pressure (GPa)	Mg#	Log ( $f_{O_2}$ ) QFM	$\Delta \log (f_{O_2})$ (cf. QFM)	Modal mineralogies (OI/Opx/Cpx/Gt)
Kaapvaal	100	3.31	740	3.00	92.3	-10.83	-2	65.5/26.9/6.1/1.3
	150	3.36	1010	4.63	91.0	-5.75	-3	65.5/26.9/6.1/1.3
	200	3.38	1250	6.28	89.0	-2.75	-4	65.5/26.9/6.1/1.3
Central Slave	100	3.28	645	2.99	93.5	-13.33	-2	75/23/0/2
	150	3.37	875	4.62	92.0	-8.00	-3	75/23/0/2
	200	3.45	1125	6.28	90.2	-4.19	-4	73/20/3/4

**Table 7**

Bulk and shear moduli, density, compressional, bulk and shear velocities (derived) and conductivity for mantle minerals at pressures and temperatures beneath the Kaapvaal and Slave cratons

Kaapvaal craton							
100 km, 740 °C, 3.00 GPa, Mg# 92.3	K (GPa)	$\mu$ (GPa)	$\rho$ (g/cm <sup>3</sup> )	Vp (km/s)	Vb (km/s)	Vs (km/s)	Log ( $\sigma$ ) (S/m)
Ol	123.43	66.99	3.31	8.01	6.11	4.50	-5.20
Opx	111.36	67.64	3.27	7.86	5.84	4.56	-5.24
Cpx	92.85	56.41	3.31	7.13	5.30	4.13	-6.05
Gt	165.84	87.55	3.62	8.83	6.77	4.92	-6.33
150 km, 1010 °C, 4.63 GPa, Mg# 91.0	K (GPa)	$\mu$ (GPa)	$\rho$ (g/cm <sup>3</sup> )	Vp (km/s)	Vb (km/s)	Vs (km/s)	Log ( $\sigma$ ) (S/m)
Ol	125.41	65.30	3.33	7.99	6.14	4.43	-3.76
Opx	121.51	67.01	3.28	8.02	6.09	4.52	-3.35
Cpx	89.51	53.63	3.31	6.97	5.20	4.02	-4.10
Gt	168.48	87.39	3.63	8.86	6.81	4.90	-4.15
200 km, 1250 °C, 6.28 GPa, Mg# 89.0	K (GPa)	$\mu$ (GPa)	$\rho$ (g/cm <sup>3</sup> )	Vp (km/s)	Vb (km/s)	Vs (km/s)	Log ( $\sigma$ ) (S/m)
Ol	127.89	63.70	3.35	7.97	6.18	4.36	-2.85
Opx	132.42	66.77	3.29	8.20	6.34	4.50	-2.24
Cpx	86.65	51.11	3.32	6.83	5.11	3.92	-2.94
Gt	171.82	87.57	3.65	8.89	6.86	4.90	-2.84
Slave craton							
100 km, 645 °C, 2.99 GPa, Mg# 93.5	K (GPa)	$\mu$ (GPa)	$\rho$ (g/cm <sup>3</sup> )	Vp (km/s)	Vb (km/s)	Vs (km/s)	Log ( $\sigma$ ) (S/m)
Ol	125.11	68.78	3.30	8.11	6.16	4.57	-5.98
Opx	113.95	68.77	3.27	7.95	5.90	4.60	-6.16
Cpx	93.92	57.43	3.30	7.19	5.33	4.17	-7.02
Gt	167.67	88.48	3.61	8.89	6.82	4.95	-7.57
150 km, 875 °C, 4.62 GPa, Mg# 92.0	K (GPa)	$\mu$ (GPa)	$\rho$ (g/cm <sup>3</sup> )	Vp (km/s)	Vb (km/s)	Vs (km/s)	Log ( $\sigma$ ) (S/m)
Ol	127.85	67.59	3.32	8.11	6.21	4.51	-4.43
Opx	125.19	68.62	3.27	8.14	6.19	4.58	-4.18
Cpx	91.13	55.04	3.31	7.05	5.25	4.08	-4.96
Gt	171.11	88.73	3.63	8.93	6.87	4.95	-5.15
200 km, 1125 °C, 6.28 GPa, Mg# 90.2	K (GPa)	$\mu$ (GPa)	$\rho$ (g/cm <sup>3</sup> )	Vp (km/s)	Vb (km/s)	Vs (km/s)	Log ( $\sigma$ ) (S/m)
Ol	130.23	65.98	3.34	8.09	6.24	4.45	-3.30
Opx	136.03	68.27	3.28	8.32	6.44	4.56	-2.77
Cpx	88.12	52.43	3.31	6.91	5.16	3.98	-3.49
Gt	174.29	88.82	3.64	8.97	6.92	4.94	-3.47

The bulk rock values are listed in Table 8. Also listed in Table 8 are the geometric means (GAV) of the values, derived by taking the geometric mean of the smallest (HS<sup>-</sup>, S=0) and largest (HS<sup>+</sup>, S=1) values.

From Table 8 one can infer that if the two cratons were juxtaposed, there would be significant differences between them at a depth of 100 km, measurable differences at 150 km (more below), but virtually no measurable differences at the base of the two lithospheres at 200 km.

**Table 8**

Upper and lower Hashin–Shtrikman bounds and geometrical averages for physical properties of mantle mineral assemblages for the Kaapvaal and Slave cratons at depths of 100 km, 150 km and 200 km

	Vp (km/s)			Vs (km/s)			Log ( $\sigma$ ) (S/m)		
	HS <sup>-</sup>	HS <sup>+</sup>	GAV	HS <sup>-</sup>	HS <sup>+</sup>	GAV	HS <sup>-</sup>	HS <sup>+</sup>	GAV
100 km									
Kaapvaal S=0	7.915	7.918	7.947	4.489	4.489	4.494	-5.314	-5.248	-5.260
Kaapvaal S=1	7.979	7.980	7.980	4.499	4.499	4.499	-5.215	-5.207	-5.207
Slave S=0	8.102	8.104	8.107	4.591	4.591	4.585	-6.125	-6.034	-6.061
Slave S=1	8.112	8.113	8.113	4.580	4.580	4.580	-6.005	-5.998	-5.998
150 km									
Kaapvaal S=0	7.891	7.894	7.915	4.405	4.406	4.409	-3.689	-3.656	-3.690
Kaapvaal S=1	7.940	7.940	7.940	4.414	4.414	4.414	-3.714	-3.692	-3.692
Slave S=0	8.059	8.060	8.050	4.498	4.500	4.490	-4.399	-4.376	-4.403
Slave S=1	8.041	8.041	8.041	4.482	4.482	4.482	-4.414	-4.408	-4.408
200 km									
Kaapvaal S=0	7.915	7.920	7.932	4.348	4.349	4.350	-2.691	-2.628	-2.704
Kaapvaal S=1	7.948	7.949	7.949	4.353	4.353	4.353	-2.760	-2.718	-2.718
Slave S=0	7.991	7.996	7.978	4.398	4.400	4.388	-3.186	-3.141	-3.210
Slave S=1	7.965	7.965	7.965	4.379	4.379	4.379	-3.255	-3.234	-3.234

7.1. Properties at 150 km depth

A particular focus is the depth of 150 km, which is approximately the top of the graphite–diamond stability field for both cratons (Kennedy and Kennedy, 1976). In addition, it is approximately the depth of the base of the ultra-depleted region beneath the Slave

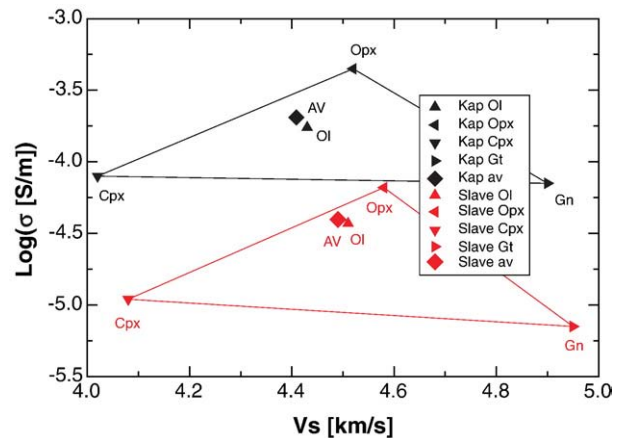


**Fig. 1.** The conductivity–Vs velocity cross-plot for minerals, and their geometrically averaged parameters, at depths of 150 km beneath the Slave (red) and Kaapvaal (black) cratons. The diamonds are the composite geometric means. The fields shown are the Opx–Cpx–Gt fields at the two temperatures and pressures. Olivine is at the apex of the tetrahedron. (For interpretation of the references to color in this figure legend, the reader is referred to the web version of this article.)

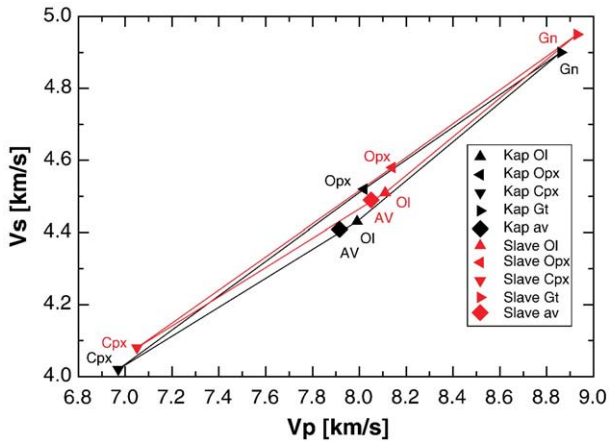


**Fig. 2.** The  $V_p$ – $V_s$  velocities cross-plot for minerals, and their geometrically averaged parameters, at depths of 150 km beneath the Slave (red) and Kaapvaal (black) cratons. The diamonds are the composite geometric mean. The fields shown are the Opx–Cpx–Gt fields at the two temperatures and pressures. Olivine is at the apex of the tetrahedron. (For interpretation of the references to color in this figure legend, the reader is referred to the web version of this article.)

craton (see below). The parameters for the individual minerals and constructed rocks at that depth are shown in Figs. 1 and 2. Fig. 1 is a cross-plot of conductivity against shear wave velocity ( $\sigma$ – $V_s$ ), and Fig. 2 shows the cross-plot of the two velocities ( $V_p$ – $V_s$ ) against each other. Clearly, conductivity has the potential to be a far greater discriminant than either of the velocities. The two tetrahedra for the velocities overlap each other considerably, whereas the tetrahedra for  $\sigma$ – $V_s$  do not. This is because of the exponential effect that temperature has on conductivity, compared to the linear dependence that applies to seismic velocities. However, determining conductivity to the required precision demands very high quality surveying techniques and also areas that are relatively free of local distortions and crustal conductors.

One can ask what the relative contribution to the conductivity and velocity difference is between the Slave values and the Kaapvaal ones based on variation in pressure, temperature, Mg#, density and composition. The pressure difference is minimal (4.62 GPa cf. 4.63 GPa), so is ignored for this comparison. Figs. 3 and 4 show the variations of conductivity and shear-wave velocity when varying all three parameters (temperature, Mg# and composition, with density given by the sum of the fractional estimates for each mineral)

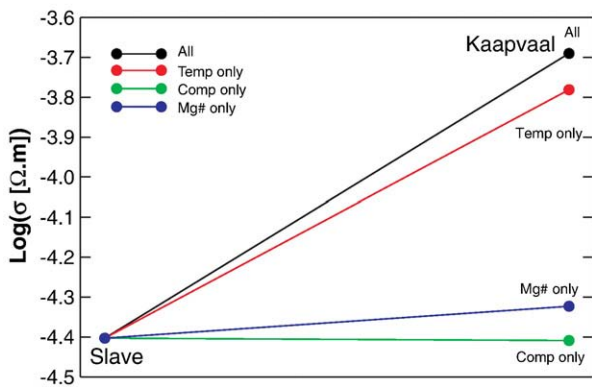


**Fig. 3.** Variation of electrical conductivity from Slave conditions to Kaapvaal conditions at 150 km depth. Black line: All three parameters changed. Red line: Only temperature changed, from 875 °C (Slave) to 1010 °C (Kaapvaal); Blue line: only Mg# changed, from 92.0 (Slave) to 91.0 (Kaapvaal). Green line: only composition (and density) changed, from 75/23/0/2 (Slave, Ol/Opx/Cpx/Gn) to 65.5/26.9/6.1/1.3 (Kaapvaal). (For interpretation of the references to color in this figure legend, the reader is referred to the web version of this article.)

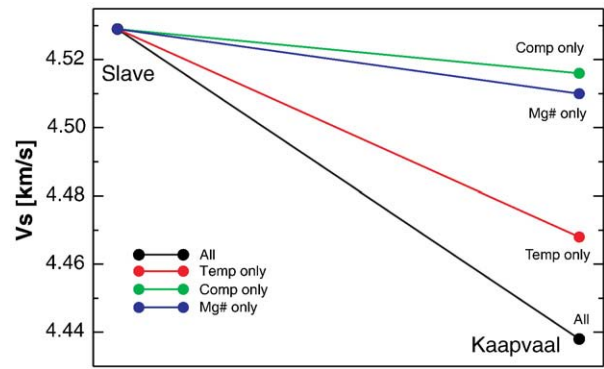


**Fig. 4.** Variation of shear wave velocity from Slave conditions to Kaapvaal conditions at 150 km depth. Black line: All three parameters changed. Red line: Only temperature changed, from 875 °C (Slave) to 1010 °C (Kaapvaal); Blue line: only Mg# changed, from 92.0 (Slave) to 91.0 (Kaapvaal). Green line: only composition (and density) changed, from 75/23/0/2 (Slave, Ol/Opx/Cpx/Gn) to 65.5/26.9/6.1/1.3 (Kaapvaal). (For interpretation of the references to color in this figure legend, the reader is referred to the web version of this article.)

simultaneously from Slave to Kaapvaal values, and the other three curves on each plot show the consequence of changing only one of the three. Temperature varies from 875 °C (Slave) to 1010 °C (Kaapvaal), Mg# from 92.0 (Slave) to 91.0 (Kaapvaal), and composition from 75/23/0/2 (Slave, Ol/Opx/Cpx/Gn) to 65.5/26.9/6.1/1.3 (Kaapvaal). Not shown are the variations in compressional or bulk velocity, as they mimic the shear-wave velocity in character, except that composition has a slightly larger effect than Mg#, compared to shear-wave velocity where it has a slightly lower effect.

One clear conclusion to be drawn from Figs. 3 and 4 is that temperature variation has the greatest effect on the physical observables of conductivity and seismic velocities. Composition variation from Slave to Kaapvaal values has virtually no effect on electrical conductivity, and an effect on velocity close to that of Mg# variation.

**Table 9**

Variation across the Hz/Lh boundary at 160 km beneath the Slave craton

Parameter	Hz layer	Lh layer
Assumed parameters		
Pressure (GPa)		4.95
Temperature (°C)		1000.0
Mg#	93.5	90.2
Ol %	75.0	73.0
Opx %	23.0	20.0
Cpx %	0.0	3.0
Gt %	2.0	4.0
P (g/cm <sup>3</sup> )	3.312	3.338
Derived parameters		
K GAV(HS <sup>−</sup> (0)–HS <sup>+</sup> (1))	127.20	126.77
G GAV(HS <sup>−</sup> (0)–HS <sup>+</sup> (1))	67.30	66.08
V <sub>p</sub> GAV(HS <sup>−</sup> (0)–HS <sup>+</sup> (1)) (km/s)	8.093	8.023
V <sub>b</sub> GAV(HS <sup>−</sup> (0)–HS <sup>+</sup> (1)) (km/s)	6.197	6.163
V <sub>s</sub> GAV(HS <sup>−</sup> (0)–HS <sup>+</sup> (1)) (km/s)	4.507	4.449
P-wave impedance	26.80	26.78
B-wave impedance	20.53	20.57
S-wave impedance	14.93	14.85
Log( $\sigma$ ) GAv(HS <sup>−</sup> (0)–HS <sup>+</sup> (1)) ( $\Omega$ m)	−3.822	−3.706
P-wave impedance contrast		−0.02
B-wave impedance contrast		+0.04
S-wave impedance contrast		−0.08
P-wave reflection coefficient		−0.0004
B-wave reflection coefficient		+0.001
S-wave reflection coefficient		−0.0027
Conductivity contrast		0.116

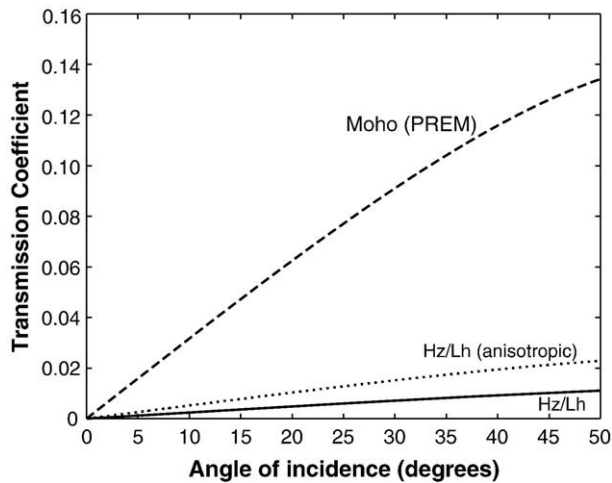


**Fig. 5.** Plane-wave P-S transmission coefficient versus incident angle for the Moho (using values for PREM; Dziewonski and Anderson, 1981) and the Hz/Lh boundary in Table 9, showing the much larger expected amplitude of the former in teleseismic receiver functions. For an epicentral distance range of 30–90°, the angle of incidence of teleseismic P waves will vary from c. 40° to 20°. The maximum plausible effect of seismic anisotropy on the transmissivity of a Hz/Lh is a factor of ~2, assuming that the Lh layer is characterized by a 4% P-wave anisotropy and a 8% S-wave anisotropy, and that the fastest anisotropic direction is coincident with the polarization and azimuth of the incident wave.

## 7.2. Harzburgite/Lherzolite boundary beneath the Slave craton

Given the observation of a boundary in teleseismic receiver functions (Snyder et al., 2004) that appears to correlate with the petrologically-determined base of the ultra-depleted harzburgitic region (Griffin et al., 1999; Menzies et al., 2004) in the centre of the Slave craton, we can construct rocks using our mineral physics knowledge and mixing relations to see if they are consistent. When we do this (Table 9), we find that there should not be an observable seismic response at all, as suggested by the negligibly small impedance contrast. Based on laboratory petrophysical data and mixing laws, others have also noted that there should be little difference in seismic velocity due to compositional variations (e.g., Goes et al., 2000; Schutt and Leshner, 2005), but the observation exists notwithstanding our theories.

Fig. 5 compares the plane-wave transmission coefficient for this boundary (Hz/Lh) with that for the Moho, computed using the model PREM (Dziewonski and Anderson, 1981) as a function of incidence angle. Note that for teleseismic P waves in the epicentral distance range of 30–90°, the angle of incidence will vary from c. 40° to 20°. In this range, the transmission coefficient for the Moho (which is typically well imaged by receiver functions) is in the range of 0.06–0.12, whereas for the Hz/Lh boundary the transmission coefficient is much smaller (0.005–0.009). Under certain assumptions about anisotropy of the medium, it may be possible to increase the transmission coefficient by a factor of ~2 (see legend of Fig. 5), but that is still insufficient to explain the observation.

## 8. Discussion and conclusions

We have constructed rocks from olivine, ortho- and clinopyroxene and garnet at appropriate temperatures and pressures for three different depths within the lithospheres of the Slave and Kaapvaal cratons. The mineral modal fractions are based on petrological observations from xenoliths in the Kimberley region of the Kaapvaal craton, and the Lac de Gras region in the central Slave craton. From laboratory determinations of the bulk and shear moduli and electrical conductivity of single crystals, we have determined bulk rock properties based on multi-phase Hashin–Shtrikman extremal bounds.

From these estimates, we determine the geometrical means, and take those for comparison.

We have ignored many effects, such as pressure and temperature dependence of moduli for the pyroxenes, hydrogen content on conductivity, pressure effects on conductivity, oxygen fugacity on conductivity, anisotropy, etc., because either these should be second order, or the laboratory data are lacking. One effect that we recognise does likely cause measurable differences is grain size, but for electrical conductivity the results of ten Grotenhuis et al. (2004) are controversial. The seismic response to grain size is most likely to arise from olivine rheology. At small grain size, low stress level, or both, mantle creep is accommodated by diffusion creep, which does not produce seismic anisotropy. Conversely, at large grain size, high stress level or both, mantle creep is dominated by dislocation creep (Karato and Wu, 1993; Eaton et al., 2009–this volume). The boundary between the two creep regimes could lead to a boundary in both grain size and seismic anisotropy that might potentially be detectable.

Within the limited range of compositions considered, i.e., those appropriate for cratonic lithosphere, temperature is the dominant factor controlling both compressional and shear wave seismic velocities and electrical conductivity. Given the exponential dependence of conductivity on temperature, it is far more sensitive than are seismic velocities. Iron content and composition are second-order effects; in fact at a depth of 150 km, conductivity is independent of the compositional variation between the Slave and Kaapvaal lithospheres.

Between the Slave and Kaapvaal cratons, at 150 km we determine a conductivity difference of more than 2/3 of an order of magnitude (log ( $\sigma$ ) of  $-4.40$  cf.  $-3.69$ ), a shear-wave velocity difference of almost 2% (4.490 cf. 4.409 km/s), and a compressional-wave velocity difference of 1.6% (8.050 cf. 7.915 km/s), for a temperature difference of 160 °C. Given that MT measurements are reliable to about 1/10th of a decade, and velocities to about 0.5%, this implies that conductivity has a temperature sensitivity of about 25 °C, Vs of about 40 °C, and Vp about 55 °C. Provided that temperature is known to this precision, then conductivity can give the Mg# to within 0.25, and the seismic velocities will give Mg# to 0.35 and compositional differences to within some 10%. Taken together, the conductivity can constrain the Mg#, thereby reducing the uncertainty in the composition to about 5%.

Perhaps our most surprising result is that based on available mineral physics data a contrast between a harzburgitic and lherzolitic mantle should not be detectable seismically, and only marginally in conductivity. Certainly the former is contrary to published observation (Snyder et al., 2004). However, Snyder et al. (2004) and Snyder and Bruneton (2007) present evidence that this interface is between two anisotropic layers with different directions of anisotropy in each: a weakly-anisotropic (3%) N–S trending upper layer overlying a more strongly anisotropic (10%) NE–SW trending lower lithospheric layer, possibly with an isotropic layer in between. Although in our examination we have only considered isotropic rocks, we have derived the expected transmission coefficient for an isotropic layer over an anisotropic one, and found that, at best, a coefficient of 0.02 can be expected, and in reality much lower (Fig. 5). Thus, including also anisotropy does not explain the large value apparent on the receiver-function data, so we have a fundamental dichotomy the requires further study.

## Acknowledgments

We wish to gratefully acknowledge the welcome advice, encouragement and support from Herman Grütter as we tried to understand the petrological aspects of this work. We thank the organizers of the Merrickville workshop for their efforts and foresight, and especially thank Nick Arndt for his patience as editor as we completed this work. S. Goes, F. Gaillard and a third reviewer provided substantial comments that improved this paper.

## References

- Afonso, J.C., Ranalli, G., Fernandez, M., 2005. Thermal expansivity and elastic properties of the lithospheric mantle: results from mineral physics of composites. *Physics of the Earth and Planetary Interiors* 149, 279–306.
- Bagdassarov, N.S., Kopylova, M.G., Eichert, S., 2007. Laboratory derived constraints on electrical conductivity beneath Slave craton. *Physics of the Earth and Planetary Interiors* 161, 126–133. doi:10.1016/j.pepi.2007.01.001.
- Ballhaus, C., 1993. Redox states of lithospheric and asthenospheric upper mantle. *Contributions to Mineralogy and Petrology* 114, 341–348.
- Beran, A., Libowitzky, E., 2006. Water in natural mantle minerals II: olivine, garnet and accessory minerals. *Reviews of Mineralogy and Petrology* 62, 169–191.
- Berryman, J.G., 1995. Mixture theories for rock properties. In: Ahrens, T.J. (Ed.), *Rock Physics and Phase Relations: A Handbook of Physical Constants*. American Geophysical Union, Washington.
- Berryman, J.G., 2006. Effective medium theories for multicomponent poroelastic composites. *ASCE Journal of Engineering Mechanics* 132, 519–531.
- Bousquet, R., Goffe, B., Le Pichon, X., de Capitani, C., Chopin, C., Henry, P., 2005. Comment on “Subduction factory: 1. Theoretical mineralogy, densities, seismic wave speeds, and H<sub>2</sub>O contents”. In: Hacker, B.R., Abers, G.A., Peacock, S.M. (Eds.), *Journal of Geophysical Research* 110, B02206. doi:10.1029/2004JB003450.
- Boyd, F.R., Pearson, D.G., Mertzman, S.A., 1999. Spinel-facies peridotites from the Kaapvaal Root. In: Gurney, J.J., et al. (Ed.), *Red Roof Design. Proceedings of the VIIth International Kimberlite Conference*, vol. 1. Cape Town, South Africa, pp. 40–48.
- Cammarano, F., Goes, S., Vacher, P., Giardini, D., 2003. Inferring upper-mantle temperatures from seismic velocities. *Physics of the Earth and Planetary Interiors* 138, 197–222.
- Carcione, J.M., Ursin, B., Nordskog, J.I., 2007. Cross-property relations between electrical conductivity and the seismic velocity of rocks. *Geophysics* 72, E193–E204.
- Chen, G., Spletzler, H.A., Getting, I.C., Yoneda, A., 1996. Selected elastic moduli and their temperature derivatives for olivine and garnet with different Mg/(Mg+Fe) contents: results from GHz ultrasonic interferometry. *Geophysical Research Letters* 23, 5–8.
- Collins, M.D., Brown, J.M., 1998. Elasticity of an upper mantle clinopyroxene. *Physics and Chemistry of Minerals* 26, 7–13.
- Constable, S.C., 2006. SEO3: a new model of olivine electrical conductivity. *Geophysical Journal International* 166, 435–437.
- Constable, S., Roberts, J.J., 1997. Simultaneous modeling of thermopower and electrical conduction in olivine. *Physics and Chemistry of Minerals* 24, 319–325.
- Constable, S., Shankland, T.J., Duba, A., 1992. The electrical conductivity of an isotropic olivine mantle. *Journal of Geophysical Research* 97, 3397–3404.
- Cox, H.L., 1952. The elasticity and strength of paper and other fibrous materials. *British Journal of Applied Physics* 3, 72–79.
- Duba, A.G., 1976. Are laboratory electrical conductivity data relevant to the Earth? *Acta Geodaetica, Geophysica et Montanistica Academiae Scientiarum Hungaricae* 11, 485–495.
- Duba, A.G., Nicholls, A., 1973. The influence of oxidation state on the electrical conductivity of olivine. *Earth and Planetary Science Letters* 18, 59–64.
- Du Frane, W.L., Roberts, J.J., Toffelmier, D.A., Tyburczy, J.A., 2005. Anisotropy of electrical conductivity in dry olivine. *Journal of Geophysical Research* 32, L24315. doi:10.1029/2005GL023879.
- Dziewonski, A., Anderson, D., 1981. Preliminary reference Earth model. *Physics of the Earth and Planetary Interiors* 25, 297–356.
- Eaton, D., Darbyshire, F., Evans, R., Grütter, H., Jones, A.G., Yuan, X., 2009. The elusive lithosphere–asthenosphere boundary beneath cratons. *Lithos* 109, 1–22 (this volume).
- Evans, R.L., Hirth, G., Baba, K., Forsyth, D., Chave, A.D., Mackie, R., 2005. Geophysical evidence from the MELT area for compositional controls on oceanic plates. *Nature* 437, 249–252.
- Farver, J.R., Yund, R.A., Rubie, D.C., 1994. Magnesium grain boundary diffusion in forsterite aggregates at 1000° – 1300 °C and 0.1 MPa to 10 GPa. *Journal of Geophysical Research* 99, 19,809–19,819.
- Ferguson, I.J., Craven, J.A., Kurtz, R.D., Boerner, D.E., Bailey, R.C., Wu, X., Orellana, M.R., Spratt, J., Wennberg, G., Norton, M., 2005. Geoelectric response of Archean lithosphere in the western Superior Province, central Canada. *Physics of the Earth and Planetary Interiors* 150, 123–143.
- Finnerty, A.A., Boyd, F.R., 1987. Thermobarometry for garnet peridotites: basis for the determination of thermal and compositional structure of the upper mantle. In: *Mantle Xenoliths*, P.H., Nixon (Eds.), Wiley & Sons, pp. 381–402.
- Flesch, L.M., Li, B., Liebermann, R.C., 1998. Sound velocities of polycrystalline MgSiO<sub>3</sub>-orthopyroxene to 10 GPa at room temperature. *American Mineralogist* 83, 444–450.
- Frederiksen, A.W., Ferguson, I.J., Eaton, D., Miong, S.-K., Gowan, E., 2006. Mantle fabric at multiple scales across an Archean–Proterozoic boundary, Grenville Front, Canada. *Physics of the Earth and Planetary Interiors* 58, 240–263.
- Gaillard, F., Bromiley, F.A., Bromiley, G.D., Rubie, D.C., Poe, B.T., 2003. Mapping water distribution in the Earth's mantle by combining geophysical and laboratory methods. *Annual Report*, 3.6.h., Bayrisches Geoinstitut.
- Gibiansky, L.V., Milton, G.W., 1993. On the effective viscoelastic moduli of two-phase media. I. Rigorous bounds on the complex bulk modulus. *Proceedings of the Royal Society of London Series A* 440, 163–188.
- Gibiansky, L.V., Torquato, S., 1993. Link between the conductivity and elastic moduli of composite materials. *Physics Reviews Letters* 71, 2927–2930.
- Gibiansky, L.V., Torquato, S., 1996. Connection between the conductivity and bulk modulus of isotropic composite materials. *Proceedings of the Royal Society of London, Series A* 452, 253–283.
- Goes, S., Govers, R., Vacher, P., 2000. Shallow mantle temperatures under Europe from P and S wave tomography. *Journal of Geophysical Research* 105, 11, 153–11,169.
- Grant, K., Ingrin, J., Lorand, J.P., Dumas, P., 2007. Water partitioning between mantle minerals from peridotite xenoliths. *Contributions to Mineralogy and Petrology* 154, 15–34.
- Griffin, W.L., Doyle, B.J., Ryan, C.G., Pearson, N.J., O'Reilly, S., Davies, R., Kivi, K., van Achtebergh, E., Natapov, L.M., 1999. Layered mantle lithosphere in the Lac de Gras area, Slave craton: composition, structure and origin. *Journal of Petrology* 40, 705–727.
- Grütter, H.S., Apter, D.B., Kong, J., 1999. Crust–mantle coupling; evidence from mantle-derived xenocrystic garnets. In: Dawson, J.B. (Ed.), *Contributed paper at: The 7th International Kimberlite Conference Proceeding*, vol. 1, pp. 307–313.
- Hacker, B.R., Abers, G.A., 2004. Subduction factory 3: an Excel worksheet and macro for calculating the densities, seismic wave speeds, and H<sub>2</sub>O contents of minerals and rocks at pressure and temperature. *Geochemistry, Geophysics, and Geosystems* 5, Q01005. doi:10.1029/2003GC000614.
- Hacker, B.R., Abers, G.A., Peacock, S.M., 2003. Subduction factory 1: theoretical mineralogy, densities, seismic wave speeds, and H<sub>2</sub>O contents. *Journal of Geophysical Research* 108 (B1), 2029. doi:10.1029/2001JB001127.
- Hacker, B.R., Abers, G.A., Peacock, S.M., Johnson, S., 2005. Reply to comment by R. Bousquet et al. on “Subduction factory: 1. Theoretical mineralogy, densities, seismic wave speeds and H<sub>2</sub>O contents”. *Journal of Geophysical Research* 110, B02207. doi:10.1029/2004JB003490.
- Hashin, Z., 1970. Theory of composite materials. In: *Wendt, F.W., Liebowitz, H., Pertone, N. (Eds.), Mechanics of Composite Materials, 5th Symposium on Naval Structural Mechanics*. Pergamon, New York, pp. 201–242.
- Hashin, Z., Shtrikman, S., 1962a. A variational approach to the theory of the effective magnetic permeability of multiphase materials. *Journal of Applied Physics* 33, 3125–3131.
- Hashin, Z., Shtrikman, S., 1962b. A variational approach to the theory of the elastic behaviour of polycrystals. *Journal of the Mechanics and Physics of Solids* 10, 343–352.
- Hashin, Z., Shtrikman, S., 1963. A variational approach to the theory of the elastic behaviour of multiphase materials. *Journal of the Mechanics and Physics of Solids* 11, 12–140.
- Hill, R., 1952. Elastic properties of reinforced solids: some theoretical principles. *Proceedings of the Physics Society of London Series A* 65, 349–354.
- Hinze, E., Will, G., Cemič, L., 1981. Electrical conductivity measurements on synthetic olivines and on olivine, enstatite, and diopside from Dreiser Weiher, Eifel (Germany) under defined thermodynamic activities as a function of temperature and pressure. *Physics of the Earth and Planetary Interiors* 25, 245–254.
- Hirsch, L.M., Shankland, T.J., 1993. Quantitative olivine-defect chemical model: insights on electrical conduction, diffusion, and the role of Fe content. *Geophysical Journal International* 114, 21–35.
- Hirsch, L.M., Shankland, T.J., Duba, A.G., 1993. Electrical conduction and polaron mobility in Fe-bearing olivine. *Geophysical Journal International* 114, 36–44.
- Hirth, G., Evans, R.L., Chave, A.D., 2000. Comparison of continental and oceanic mantle electrical conductivity: is the Archean lithosphere dry. *Geochemistry, Geophysics, and Geosystems* 1, 2000GC000048.
- Ingrin, J., Blanchard, M., 2006. Diffusion of hydrogen in minerals. *Reviews in Mineralogy and Geochemistry* 62, 291–320.
- Isaak, D.G., 1993. High-temperature elasticity of iron-bearing olivines. *Journal of Geophysical Research* 97, 1871–1885.
- Isaak, D.G., Ohno, I., Lee, P.C., 2006. The elastic constants of monoclinic single-crystal chrome-diopside to 1,300 K. *Physics and Chemistry of Minerals* 32, 691–699.
- Jackson, J.M., Sinogeikin, S.V., Bass, J.D., 2007. Sound velocities and single-crystal elasticity of orthoenstatite to 1073 K at ambient pressure. *Physics of the Earth and Planetary Interiors* 161, 1–12.
- James, D.E., Boyd, F.R., Schutt, D., Bell, D.R., Carlson, R.W., 2004. Xenolith constraints on seismic velocities in the upper mantle beneath southern Africa. *Geochemistry, Geophysics, and Geosystems* 5, Q01002. doi:10.1029/2003GC000551.
- Jaupart, C., Mareschal, J.C., 1999. The thermal structure and thickness of continental roots. *Lithos* 48, 93–114.
- Ji, S., Wang, S., 1999. Elastic properties of forsterite–enstatite composites up to 3.0 GPa. *Geodynamics* 28, 147–174.
- Ji, S., Wang, Q., Xia, B., Marcotte, D., 2004. Mechanical properties of multiphase materials and rocks: a phenomenological approach using generalized means. *Journal of Structural Geology* 26, 1377–1390.
- Jiang, F., Speziale, S., Shieh, S.R., Duffy, T.S., 2004. Single-crystal elasticity of andradite garnet to 11 GPa. *Journal of Physics of Condensed Matter* 16, S1041–S1052.
- Jones, A.G., Craven, J.A., 2004. Area selection for diamond exploration using deep-probing electromagnetic surveying. *Lithos* 77, 765–782.
- Jones, A.G., Lezaeta, P., Ferguson, I.J., Chave, A.D., Evans, R.L., Garcia, X., Spratt, J., 2003. The electrical structure of the Slave craton. *Lithos* 71, 505–527.
- Jones, M.Q.W., 1988. Heat flow in the Witwatersrand Basin and environs and its significance for the South African shield geotherm and lithosphere thickness. *Journal of Geophysical Research* 93, 3243–3260.
- Karato, S., 1990. The role of hydrogen in the electrical conductivity of the upper mantle. *Nature* 347, 272–273.
- Karato, S., 2006. Remote sensing of hydrogen in Earth's mantle. *Reviews of Mineralogy and Geochemistry* 62, 343–375.
- Karato, S., Wu, P., 1993. Rheology of the upper mantle: a synthesis. *Science* 260, 771–778.
- Katsura, T., Yokoshi, S., Kawabe, K., Shatskiy, A., Okube, M., Fukui, H., Ito, E., Nozawa, A., Funakoshi, K.-I., 2007. Pressure dependence of electrical conductivity of (Mg,Fe) SiO<sub>3</sub> ilmenite. *Physics and Chemistry of Minerals* 34, 249–255. doi:10.1007/s00269-007-0143-0.
- Kelly, R.K., Kelemen, P.B., Jull, M., 2003. Buoyancy of the continental upper mantle. *Geochemistry, Geophysics, and Geosystems* 4, 1017. doi:10.1029/2002GC000399.

- Kennedy, C.S., Kennedy, G.C., 1976. The equilibrium boundary between graphite and diamond. *Journal of Geophysical Research* 81, 2467–2470.
- Kohlstedt, D., Mackwell, S., 1998. Diffusion of hydrogen and intrinsic point defects in olivine. *Zeitschrift für Physikalische Chemie. (International Journal of Research in Physical Chemistry and Chemical Physics)* 207, 147–162.
- Kopylova, M.G., Caro, G., 2004. Mantle xenoliths from the southeastern Slave craton: the evidence for a thick cold stratified lithosphere. *Journal of Petrology* 45, 1045–1067.
- Kopylov, M.G., Lo, J., Christensen, N.I., 2004. Petrological constraints on seismic properties of the Slave upper mantle (Northern Canada). *Lithos* 77, 493–510. doi:10.1016/j.lithos.2004.03.012.
- Kopylova, M.G., Russell, J.K., 2000. Composition and stratification of the Slave cratonic upper mantle. *Earth and Planetary Science Letters* 181, 71–87.
- Kronrod, V.A., Kuskov, O.L., 2007. Modeling of the thermal structure of continental lithosphere. *Izvestiya, Physics of the Solid Earth* 43, 91–101.
- Kuskov, O.L., Kronrod, V.A., Annersten, H., 2006. Inferring upper-mantle temperatures from seismic and geochemical constraints: implications for Kaapvaal craton. *Earth and Planetary Science Letters* 244, 133–154.
- Ledo, J., Jones, A.G., 2005. Temperature of the upper mantle beneath the Intermontane Belt, northern Canadian Cordillera, determined from combining mineral composition, electrical conductivity laboratory studies and magnetotelluric field observations. *Earth and Planetary Science Letters* 236, 258–268.
- Lee, C.-T.A., 2003. Compositional variation of density and seismic velocities in natural peridotites at STP conditions: implications for seismic imaging of compositional heterogeneities in the upper mantle. *Journal of Geophysical Research* 108. doi:10.1029/2003JB002413.
- Li, B., Liebermann, R.C., 2007. Indoor seismology by probing the Earth's interior by using sound velocity measurements at high pressures and temperatures. *Proceedings of the National Academy of Sciences, USA*, 104, pp. 9145–9150. doi:10.1073/pnas.0608609104.
- Li, L.X., Wang, T.J., 2005. A unified approach to predict overall properties of composite materials. *Materials Characterization* 54, 49–62.
- Liu, W., Li, B., 2006. Thermal equation of state of  $(\text{Mg}_{0.9}\text{Fe}_{0.1})_2\text{SiO}_4$  olivine. *Physics of the Earth and Planetary Interiors* 157, 188–195.
- Mareschal, J.C., Nyblade, A., Perry, H.K.C., Jaupart, C., Bienfait, G., 2004. Heat flow and deep lithospheric thermal structure at Lac de Gras, Slave Province, Canada. *Geophysical Research Letters* 31, L12611. doi:10.1029/2004GL020133.
- Mareschal, M., Kellett, R.L., Kurtz, R.D., Ludden, J.N., Bailey, R.C., 1995. Archean cratonic roots, mantle shear zones and deep electrical anisotropy. *Nature* 375, 134–137.
- Maxwell-Garnett, J.C., 1904. Colours in metal glasses and in metallic films. *Philosophical Transactions of the Royal Society of London, Series A* 203, 385–420.
- McCammon, C., Kopylova, M.G., 2004. A redox profile of the Slave mantle and oxygen fugacity control in the cratonic mantle. *Contributions to Mineralogy and Petrology* 148, 55–68. doi:10.1007/s00410004-0583-1.
- Menzies, A., Westerland, K., Grütter, H., Gurney, J., Fung, A., Nowicki, T., 2004. Peridotitic mantle xenoliths from kimberlites on the Ekati Diamond Mine property, N.W.T., Canada: major element compositions and implications for the lithosphere beneath the central Slave craton. *Lithos* 77, 395–412.
- Mierdel, K., Keppler, H., Smyth, J.R., Langenhorst, F., 2007. Water solubility in aluminous orthopyroxene and the origin of Earth's asthenosphere. *Science* 315, 364–368.
- Milton, G.W., Berryman, J.G., 1997. On the effective viscoelastic moduli of two-phase media. II. Rigorous bounds on the complex shear modulus in three dimensions. *Proceedings of the Royal Society of London Series A* 453, 1849–1880.
- Myers, J., Eugster, H.P., 1983. The system Fe–Si–O: oxygen buffer calibrations to 1,500K. *Contributions to Mineralogy and Petrology* 82, 75–90.
- Nestola, F., Ballaran, T.B., Tribaudino, M., Ohashi, H., 2004. Compressional behaviour of  $\text{CaNiSi}_2\text{O}_6$  clinopyroxene: bulk modulus systematic and cation type in clinopyroxenes. *Physics and Chemistry of Minerals* 32, 222–227.
- Nover, G., 2005. Electrical properties of crustal and mantle rocks – a review of laboratory measurements and their explanation. *Surveys in Geophysics* 26, 593–651.
- O'Reilly, S.Y., Griffin, W.L., 2006. Imaging global chemical and thermal heterogeneity in the subcontinental lithospheric mantle with garnets and xenoliths: geophysical implications. *Tectonophysics* 416, 289–309.
- Park, S.K., Ducea, M.N., 2003. Can in situ measurements of mantle electrical conductivity be used to infer properties of partial melts. *Journal of Geophysical Research* 108. doi:10.1029/2002JB001899 EPM 14-1 – EPM 14-12, Art. No. 2270.
- Perrillat, J.-P., Nestola, F., Sinogeikin, S.V., Bass, J.D., 2007. Single-crystal elastic properties of  $\text{Ca}_0.07\text{Mg}_{1.93}\text{Si}_2\text{O}_6$  orthopyroxene. *American Mineralogist* 92, 109–113.
- Poe, B.T., Romano, C., Nestola, F., Rubie, D.C., 2005. Electrical conductivity of hydrous single crystal San Carlos Olivine. *Eos Transactions of the American Geophysical Union* 86 (52) Fall Meeting Supplement, Abstract MR41A-0895.
- Poudjom Djomani, Y.H., O'Reilly, S.Y., Griffin, W.L., Morgan, P., 2001. The density structure of subcontinental lithosphere through time. *Earth and Planetary Science Letters* 184, 605–621.
- Reuss, A., 1929. Berechnung der Fließgrenze von Mischkristallen auf Grund der Plastizitätsbedingung für Einkristalle. *Zeitschrift für Angewandte Mathematik und Mechanik* 9, 49–58.
- Roberts, J.J., Tyburczy, J.A., 1991. Frequency-dependent electrical-properties of polycrystalline olivine compacts. *Journal of Geophysical Research* 96, 16,205–16,222.
- Romano, C., Poe, B.T., Kreidie, N., McCammon, C.A., 2006. Electrical conductivities of pyrope-almandine garnets up to 19 GPa and 1700 °C. *American Mineralogist* 91, 1371–1377.
- Russell, J.K., Kopylova, M.G., 1999. A steady-state conductive geotherm for the north-central Slave: inversion of petrological data from the Jericho kimberlite pipe. *Journal of Geophysical Research* 104 (B4), 7089–7101.
- Salje, E.K.H., 2007. An empirical scaling model for averaging elastic properties including interfacial effects. *American Mineralogist* 92, 429–432.
- Schock, R.N., Duba, A., Shankland, T.J., 1989. Electrical conduction in olivine. *Journal of Geophysical Research* 94, 5829–5839.
- Schutt, D.L., Leshner, C.E., 2005. Effects of melt depletion on the density and seismic velocity of garnet and spinel lherzolite. *Journal of Geophysical Research* 111, B05401. doi:10.1029/2003JB002950.
- Seifert, K.F., Will, G., Voigt, R., 1982. Electrical conductivity measurements on synthetic pyroxenes  $\text{MgSiO}_3$ – $\text{FeSiO}_3$  at high pressures and temperatures under defined thermodynamic conditions. In: Schreyer, W. (Ed.), *High Pressure Researches in Geoscience*. E. Scheizerbartsche Verlagsbuchhandlung, Stuttgart, pp. 419–432.
- Shankland, T.J., Peyronneau, J., Poirier, J.P., 1993. Electrical conductivity of the Earth's lower mantle. *Nature* 366, 453–455.
- Simpson, F., 2002. Intensity and direction of lattice-preferred orientation of olivine: are electrical and seismic anisotropies of the Australian mantle reconcilable? *Earth and Planetary Science Letters* 203, 535–547.
- Simpson, F., Tommasi, A., 2005. Hydrogen diffusivity and electrical anisotropy of a peridotite mantle. *Geophysical Journal International* 160, 1092–1102.
- Snyder, D.B., Brunton, M., 2007. Seismic anisotropy of the Slave craton, NW Canada, from joint interpretation of SKS and Rayleigh waves. *Geophysical Journal International* 169, 170–188. doi:10.1111/j.1365-246X.2006.03287.x.
- Snyder, D.B., Rondenay, S., Bostock, M.G., Lockhart, G.D., 2004. Mapping the mantle lithosphere for diamond potential using teleseismic methods. *Lithos* 77, 859–872.
- Stachel, T., Harris, J.W., Tapperta, R., Brey, G.P., 2003. Peridotitic diamonds from the Slave and the Kaapvaal cratons—similarities and differences based on a preliminary data set. *Lithos* 71, 489–503.
- Stocker, R., 1978. Influence of oxygen pressure on defect concentrations in olivine with a fixed cationic ratio. *Physics of the Earth and Planetary Interiors* 17, 118–129.
- ten Grotenhuis, S.M., Drury, M.R., Peach, C.J., Spiers, C.J., 2004. Electrical properties of fine-grained olivine: evidence for grain boundary transport. *Journal of Geophysical Research* 109, B06203. doi:10.1029/2003JB002799.
- Vacher, P., Verhoeven, O., 2007. Modelling the electrical conductivity of iron-rich minerals for planetary applications. *Planetary and Space Science* 55, 455–466.
- Voigt, W., 1928. *Lehrbuch der Kristallphysik*. Teubner, Leipzig.
- Wang, D., Mookherjee, M., Xu, Y., Karato, S.-I., 2006. The effect of water on the electrical conductivity of olivine. *Nature* 443, 977–980. doi:10.1038/nature05256.
- Watt, J.P., Davies, G.F., O'Connell, R.J., 1976. The elastic properties of composite materials. *Reviews of Geophysics and Space Physics* 14, 541–563.
- Woodland, A.B., Koch, M., 2003. Variation in oxygen fugacity with depth in the upper mantle beneath the Kaapvaal craton, Southern Africa. *Earth and Planetary Science Letters* 214, 295–310.
- Xu, Y.S., Poe, B.T., Shankland, T.J., Rubie, D.C., 1998. Electrical conductivity of olivine, wadsleyite and ringwoodite under upper-mantle conditions. *Science* 280, 1415–1418.
- Xu, S., Shankland, T.J., 1999. Electrical conductivity of orthopyroxene and its high pressure phases. *Geophysical Research Letters* 26, 2645–2648.
- Xu, Y.S., Shankland, T.J., Duba, A.G., 2000a. Pressure effect on electrical conductivity of mantle olivine. *Physics of the Earth and Planetary Interiors* 118, 149–161.
- Xu, Y.S., Shankland, T.J., Poe, B.T., 2000b. Laboratory-based electrical conductivity of the Earth's mantle. *Journal of Geophysical Research* 105, 27,865–27,875.
- Vacher, P., Mocquet, A., Sotin, C., 1996. Comparison between tomographic structures and models of convection in the upper mantle. *Geophysical Journal International* 124, 45–56.
- Yi, L., Wang, D.-J., Li, H.-P., 2005. Electrical properties of natural pyroxenite. *Chinese Physics Letters* 22, 2140–2142.
- Yoshino, T., Matsuzaki, T., Yamashita, S., Katsura, T., 2006. Hydrous olivine unable to account for conductivity anomaly at the top of the asthenosphere. *Nature* 443, 973–976. doi:10.1038/nature05223.